



Potential of data centers for fast frequency response services in synchronously isolated power systems

Dlzar Al Kez^{a,b,*}, Aoife M. Foley^{c,d,e,**}, Faraedoon W. Ahmed^f, Mark O'Malley^{g,h}, S. M. Muyeenⁱ

^a School of Electronics, Electrical Engineering and Computer Science, Queen's University Belfast, Belfast, BT9 5AH, UK

^b Department of Electrical Engineering, University of Sulaimani, Sulaimaniyah, Iraq

^c Department of Civil, Structural and Environmental Engineering, Trinity College Dublin, Dublin, Ireland

^d School of Mechanical and Aerospace Engineering, Queen's University Belfast, Belfast, BT9 5AH, UK

^e Department of Mechanical Engineering, Massachusetts Institute of Technology, USA

^f College of Science, Physics Department, University of Halabja, Sulaimaniyah, Iraq

^g Energy Systems Integration Group, Virginia, 20195, USA

^h School of Electrical and Electronic Engineering, University College Dublin, Dublin 4, Ireland

ⁱ School of Electrical Engineering, Computing and Mathematical Sciences, Curtin University, Perth, WA, 6845, Australia



ARTICLE INFO

Keywords:

Demand response
Fast frequency response
Frequency transients
Internet data centers
Low inertia power systems
Uninterruptable power supply (UPS)
Wind power generation

ABSTRACT

Grid frequency support is one of the most challenging issues in wind rich islanded power systems. This problem becomes critical with the displacement of synchronous generators and their associated services (i.e., inertia and primary operating reserve). The services that are lost can be replaced by other sources, such as demand response schemes to enhance the resiliency and security of power system operations. Demand response based on internet data centers is expected to become an increasingly important asset to make a significant contribution to frequency ancillary services. To exploit this resource, internet service companies are expected to combine the capabilities of a variety of data centers to participate as a single provider similar to a virtual power plant. In this context, this work develops a novel framework for cooperative participation of data centers delay-tolerant workloads and backup power supply units to provide effective fast frequency response service. This is achieved by employing the model predictive controller to initiate reference signals to data center resources while respecting device operating conditions and constraints. Various case studies are run on the modified linear model of the 39 Bus system via dynamic simulations for the projected 75 % system non-synchronous penetration. Simulation results demonstrate the potential of different data center configurations to stabilize grid frequency during signal delays and severe cascade failures. The analysis shows that the proposed framework is critical to the adoption of renewable energy and reduces the requirement for an expensive spinning reserve used in a typical power system.

1. Introduction

Internet data centers (IDC) have emerged as major electricity consumers that accounted for 2 % of the total global final electricity demand in 2019 and are expected to reach 8 % in 2030 [1]. Data centers are anticipated to become a significant segment and major energy consumer of the Irish power system. There is currently approximately 1000 MVA contracted demand capacity to large energy consumers, primarily IDC [2]. The installed capacity of IDC infrastructure is anticipated to reach

nearly 1100, 1400 MVA, and 1900 MVA in the low, median, and high demand forecast scenarios respectively [2]. The forecasted build-out per future scenario out to 2028 is shown in Fig. 1. Analysis by Ireland's transmission system operators (TSOs) EirGrid and SONI shows that demand for IDC in the median scenario will account for 29 % of the total system electricity demand by 2028, making IDC the fastest growing energy consumption subsector [2]. However, the good news is that IDC technologies are highly automated and technically can adapt their power consumption in a fine-grained way using a variety of power management techniques at different levels of data center architecture (i.

* Corresponding author. School of Electronics, Electrical Engineering and Computer Science, Queen's University Belfast, Belfast, BT9 5AH, UK.

** Corresponding author. Department of Civil, Structural and Environmental Engineering, Trinity College Dublin, Dublin, Ireland.

E-mail addresses: dalkez01@qub.ac.uk (D. Al Kez), foleyao@tcd.ie, a.foley@qub.ac.uk (A.M. Foley).

Nomenclature	
<i>List of abbreviations</i>	
CPP	Conventional power plants
CPU	Central processing unit
DR	Demand response
DFIG	Doubly-fed induction generator
DVFS	Dynamic voltage frequency scaling
EMS	Energy management systems
FFR	Fast frequency response
HVDC	High voltage direct current
HWLI	High wind low inertia
IBR	Inverter based renewable
IDC	Internet data center
IR	Inertia response
IT	Information technology
ISC	Internet service companies
LSI	Largest single infeed
LFC	Load frequency control
LWHI	Low wind high inertia
MPC	Model predictive controller
MWMI	Medium wind medium inertia
NWHI	No wind high inertia
POR	Primary operating reserve
PV	Photovoltaics
PMU	Phasor measurement units
RoCoF	Rate of change of frequency
SNSP	System non-synchronous penetration
STAR	Short Term Active Response
SLA	Service level agreement
TSO	Transmission system operators
UFLS	Under-frequency load shedding
UPS	Uninterruptable power supply
UK	United Kingdom
VSWG	Variable speed wind generation
<i>List of symbols</i>	
GDB	Synchronous generators deadband
GRC	Generation rate constraint
K_{IRi}	RoCoF controller gain
K_{UPSi}	Fast frequency response controller gain
K_{DRi}	Demand response controller gain
K_{CCP}	Synchronous generator distribution coefficient factor
K_W	Wind farm distribution coefficient factor
ΔP_{mi}	Power generation in an Area
ΔP_{Li}	Total demand in an Area
ΔP_{wi}	Wind power generation in an Area
$\Delta P_{tie,i}$	Tie-line power flow between two adjacent Areas
ΔP_{FFR}	Volume of fast frequency response power
ΔP_{UPS}	Aggregated UPS power
ΔP_{DR}	Aggregated IT load capacity
P_{IR}	Virtual inertia response
P_{UPS}^{min}	UPS minimum power
P_{FFR}	Fast frequency power
P_{FFR}^{up}	Regulation up
P_{FFR}^{down}	Regulation down
P_{UPS}^{max}	UPS maximum power
$\Delta P_{ref}^{UPS_i}$	Reference power of a UPS in a data center
$E_{UPS}(t)$	UPS delivered energy
P_{DR}^{min}	Minimum available demand power
P_{DR}^{max}	Maximum delivered demand power
dp^+/dt	UPS ramp up rate limit
dp^-/dt	IT load ramp down rate limit
df/dt	Rate of change of frequency
Δf_i	Frequency deviation in an area
$f_{DB, CPP}$	Synchronous generator frequency deadband
$f_{DB, FFR}$	Fast frequency response deadband
f_o	Nominal system frequency
ρ	Air density
A	Swept area
C_p	Indicates power coefficient
V_w	Wind speed
λ	Tip speed ratio
β	Pitch angle
H_i	Inertia constant of an Area
D_i	Damping coefficient of an Area
N	Set of controlled Areas
M	Number of participated UPS and IT loads
α_i	Sharing factor
R_i	Synchronous generators droop coefficient
SoC_{max}	UPS maximum state of charge
SoC_{min}	UPS minimum state of charge
T_R	Response time
T_{FFR}	Sustained response time
τ_d	Delay time
τ_a	Actuation time
τ_c	Communication delay
T_{IR}	RoCoF controller time constant
T_{DRi}	IT load FFR controller time constant
T_{ij}	Tie-line synchronizing torque coefficient
U_{UPSi}	UPS control signal
U_{DRi}	IT load control signal
<i>List of SI units</i>	
kW	kilowatt
kWh	kilowatt hour
MW	Megawatt
MVA	Megavolt ampere
p.u.	per unit
Hz	Hertz
mHz	millihertz
s	second
ms	millisecond

e., hardware, workload, infrastructure, and applications) [3].

The potential expansion in the numbers and scales of IDC should be considered, especially in light of the energy system undergoing its own engineering, corporate and social changes due to government regulations for greenhouse gas emissions to combat global warming. The outcomes of the intergovernmental panel on climate change (IPCC) 2018 report were evident, globally carbon-neutral by 2055, to stand any chance of enduring by the Paris Agreement and to minimize the potential impacts of catastrophic runaway global warming [4]. It can be argued that electrical power systems are among the easiest energy

supplies to decarbonize when compared to transportation and heating. As part of the climate action plan, the European Union (EU) has set ambitious targets to produce 54 % of the gross generated electricity mix from renewable sources by 2030 [5]. Among the EU countries, Ireland has set itself the challenge of sourcing 70 % of its electricity generation from renewable energy, predominantly variable speed wind generation (VSWG) by 2030 with no generation from peat and coal [2]. The system is currently operating at 70 % system non-synchronous penetration (SNSP) [6] and there will be requirements to be able to operate with 95 % generation coming from non-synchronous resources to achieve 2030

targets [7].

The increased levels of inverter-based renewables (IBR) (i.e., wind turbines, and solar photovoltaics (PV) systems) and high voltage direct current (HVDC) interconnectors) impose new previously unseen challenges to real-time power systems operational control. This is because IBRs are not electromechanically coupled to the utility grid, and thus the inertia of their rotating mass, as in VSWG, is not exposed to the transmission network. Consequently, large penetrations of IBRs further displaces the amount of spinning mass and necessitates a significant reduction in the overall power system inertia [8]. It is this rotating mass that gives the system its property of inertia. Namely, the inertia makes the system reluctant to a change in its angular velocity, and frequency. In addition, at the grid-scale of IBR, the number of online synchronous generator units providing primary operating reserve (POR) reduces, meaning that the system is less able to handle the loss of large infeeds, and not as effective with remaining stable during significant faults [9]. Consequently, the instantaneous balance between generation, demand and power grid management in real-time is becoming a challenging task for TSOs [10].

A direct threat from low system inertia and spinning reserve is a larger and faster rate of change of frequency (RoCoF) with higher frequency deviation (nadir). Extreme RoCoF and frequency nadir are highly undesirable as they contribute to triggering the anti-islanding RoCoF protection relays followed by load shedding, which in turn may lead to cascading failures and eventually complete system blackout similar to that which occurred in the South Australia 2016 blackout [11]. Similarly, on August 9th, 2019, two power plants were tripped in the United Kingdom (UK) and consequently, system frequency reached a nadir of 48.8 Hz [12]. This resulted in triggering the under-frequency load shedding (UFLS) protocols which affected one million customers, and numerous factories and facilities.

Currently, uncertainties associated with the operation of IBR are handled by means of the spinning reserve of conventional generators [9]. However, significant penetrations of IBRs can potentially reduce interconnection frequency response if they are not operated with frequency sensitive mode. Alternative system frequency services (e.g., virtual inertia response (IR) and fast frequency response (FFR)) are being explored by countries like Ireland, UK, and Australia to securely operate the system with high IBRs [13]. The FFR aims to deploy responses with a shorter time delay (i.e., less than or equal to 2 s from the start of the event) than traditional droop-based response, thereby enhancing extreme frequency deviations [14]. Thus, if the service is provided from renewable resources or from demand response (DR) that is entirely supplied by renewable energy, it will not only be at par with

traditional regulation mechanisms in terms of efficiency but it will also be environmentally friendly.

The motivation of this analysis lies in the fact that IDCs represent a particularly promising sector for the adoption of DR programs to help create a balance in the future low inertia power grids. However, the key challenge remains the commitment of the IDC sector to drive to net-zero carbon as part of their social corporate due diligence to support grid operators and governments to achieve renewable and sustainable energy targets. The biggest hurdle to truly analyzing this opportunity, so that regulators can support such a grid support service, is the commercial sensitivity and availability of IDC operations datasets. Important questions arise are, first what data structure required to predict and control IDCs that could enable real-time IR and FFR services? What is the potential impact of IDCs in the future of frequency control as synchronous generation fraction reduces?

In this context, this research proposes a radically new approach for rebalancing frequency deviation at grid-level using the joint advantages of the on-site uninterruptable power supply (UPS) and information technology (IT) workload shifting. A model predictive control (MPC) as an optimization-based control scheme has been applied in the coordination control of different IDC resources to enhance the whole power system stability. The MPC method appears to be promising to integrate all the aforementioned aspects into a uniform problem formulation [15]. The capability of the MPC to compute optimal control signals based on predictions of future state evaluation has made it an attractive controller for IBR to provide FFR service [15,16], virtual IR response [17], and power system frequency regulations [18]. Furthermore, utilizing MPC for IDC load control has recently gained attention due to the controller capability of incorporating state-space network model and disturbance forecasts while taking the device operational constraints [19,20]. This analysis adds to the literature while particularly focuses on a framework that aims at leveraging IDCs fast response capabilities to real-time control signals, thereby managing system frequency rapidly and guaranteeing secure operation of the power system at 75 % SNSP. The main contributions of this paper are listed below:

1. A centralized MPC based FFR framework that enables internet service companies (ISC) to detect signaling from the grid and provide a coordinated response from UPS systems and IT load reduction is presented. The proposed framework can be added as an additional layer to the current frequency response services.
2. The MPC method is implemented, which can act as a catalyst to send reference signals to the IDC participants to provide reliable frequency support while respecting the IDC operational constraints. The

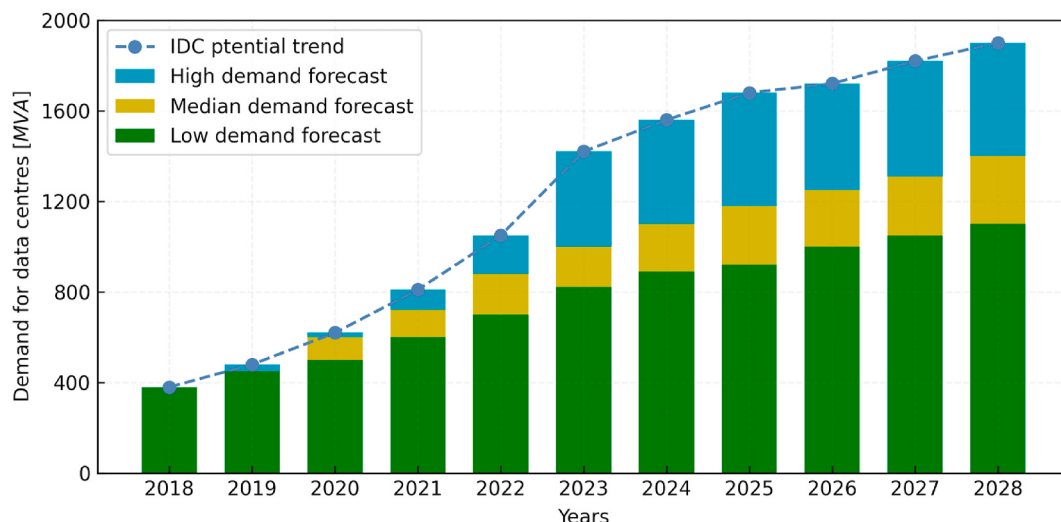


Fig. 1. The expected installed capacity from assumed build-out of IDC large energy users in Ireland.

- negative impact of the IDC operational constraints on the FFR provision is also examined.
3. Extensive sensitivity analysis is carried out emphasizing future operational dispatches with large penetration of IBRs which do not provide POR capabilities. The effectiveness of the proposed framework on the important system frequency metrics (i.e., RoCoF, nadir, time to nadir, and settling frequency), following credible and non-credible cascading disturbances, is demonstrated.
 4. The impact of uncertainties associated with the variability of wind power generation and communication delays are also investigated. The capability of the MPC controller to reject disturbances during various delay signals is assessed.

The rest of the paper is organized as follows: Section 2 presents an overview of data center participation in DR. The proposed IDC framework is given in Section 3. This is followed by the model of the IDC using the MPC method in Section 4. Simulation results and discussion are illustrated in Section 5. Section 6 concludes the work with some remarkable future directions.

2. Background study

Power consumption in IDCs can be broadly categorized into power consumed by IT equipment (i.e., servers, storage, networks) and infrastructure (i.e., cooling, lighting). In a typical data center, IT power consumption accounts for 50 % of the total power consumed [21]. This is followed by the cooling system with 35 %, electrical losses attributed to the UPS energy conversion with 11 %, and lighting with 4 %. The server power consumption can vary to some degree depending on the IT workloads. The practical use of IDC assets in the ancillary service market can be best attributed to two key reasons.

1. Data centers utilize an array of batteries with a number of redundant UPS systems that could be used to provide instantaneous grid support during disturbances.
2. The cloud of modern era IDCs can dynamically adjust their power consumption via various strategies to participate in FFR services.

2.1. Uninterruptable power supply

The primary task of the current UPS systems is to take inbound power and produce high-quality constant output power for the IT servers. Furthermore, they protect IDC critical loads during power supply failure for a very short interval of time, usually, less than 1 min until the onsite backup generators start [22]. Although the required energy for a typical IDC during disturbances is comparatively less than the installed UPS capacity [23], the current UPS systems are technically not enabled and/or utilized to provide the ancillary services to the grid.

However, if the UPS system were reconfigured and upgraded, they could provide system frequency services during disturbances. This job requires additional functionalities to be implemented in the power-electronics converters to enable them to receive control signals. There are significant efforts underway within the industry (e.g., Eaton's Energy Aware 93 M and 9395P UPS systems) to incentivize modern UPS design with bi-directional converters and in-built control algorithms that can feed power back to the grid in the event of disturbance [24]. Indeed, this idea has been proposed and examined for primary and secondary frequency response in Refs. [25,26] respectively, as well as for FFR service in our previous works in Refs. [10,27]. Nonetheless, the potential benefits from this resource are not investigated in the presence of high wind power generation which is the main focus of this research.

2.2. IT loads

The cloud of modern era IDCs can dynamically adjust their power

consumption via various strategies to participate in FFR services. The most common mechanisms amongst these modern era IDCs are workload migration [28,29], dynamic capacity provisioning [30], and dynamic voltage and frequency scaling (DVFS) [31,32]. In the former technique, the IDC power demand from one particular geographical location can be massively and discretionarily moved to another area via the data network. This offers both temporal and spatial load regulation by utilizing geographical load balancing techniques. Accordingly, the cooperative IDCs can act as an important DR resource to help ISCs reduce their energy costs.

It is essential to note that the average required time for IDC server migration could take up to 8 min [32]. Similarly, capacity provisioning deals with turning ON and OFF the computing servers to adjust the segregated power consumption of the IDCs. This method, however, requires a long actuation time as well as the ON and OFF transition process of the servers leading to higher energy consumption. Nonetheless, DVFS deals with the central processing unit (CPU) frequency alteration to minimize the server's overall power consumption. The main disadvantage of these techniques is their significant impact on the service level agreement (SLA) performance degradation in terms of average response time and job deadline violations [23].

Moreover, the majority of the existing work in IDC DR has been mainly focused on the development of mathematical algorithms for optimizing the price performance of different IDCs in the DR market. For instance, in Ref. [19] the authors performed IDC cost optimization using MPC based deferrable jobs in order to increase renewable energy usage. Furthermore, the MPC based control framework to leverage IDC cooling systems, delay-tolerant workloads and enable UPS units to participate in price-based DR services and to minimize IDC operational costs developed in Ref. [20]. At faster timescales, the joint optimization of IDC and plug-in electric vehicles (EV) for frequency regulation examined in Ref. [31]. Similarly, a synergic control strategy that combines power management of IT loads and cooling systems to provide frequency regulation using proportional, integral, and derivative controllers studied in Ref. [32], but no reference to system-level frequency studies. In another work, the potential of IDCs in the ancillary secondary frequency response services explored in Ref. [33], but again without frequency analysis.

Importantly, the main focus of literature has been on the application of IDCs on a timescale of hours or longer [34], which wastes the full capability and effectiveness of IDCs as DR resources. When the level of system inertia reduces, the timescale of interest shrinks to seconds or less. The broad goal of this analysis is to help fill this research gap that considers joint advantages of IDC load shifting and UPS systems at high wind power generation. The most tempting significance of load postponing is its instantaneous reaction time with guaranteed SLA availability [35]. As we are aiming for the FFR service, the fastest possible timescale less than 2 s, real-time workload shifting is of interest rather than CPU throttling or workload migration. Load shifting or rescheduling provides flexibility to temporarily delay non-critical workloads to future timeframes for the sake of reducing IT power consumption. The workloads in a typical cloud computing environment have flexibilities in terms of SLA (e.g., agreements of backup services do not necessarily need to be carried out instantly) when the operation should be performed. Nonetheless, they require a frequent backup operation, and their availability is maintained at a high level, such as 99.99 % [35]. Compared to other types of electric loads, IT servers are well-suited to participate in real-time frequency services because of their fine granularity controllable power consumption (not ON/OFF) with fast ramp rates [36]. However, utilizing the fundamental IT resources corresponds to the available amount of workloads that need to be completed. An empirical field study by Lawrence Berkeley National Laboratories (LBNL) [37] demonstrated that in a typical IDC, 15 % of the total IT workloads could be shifted for up to several hours.

3. Proposed IDC framework for FFR service

In the above context, a novel centralized FFR framework is developed to manage a portfolio of IDCs in a typical ISC. The proposed method is conceptually summarized in Fig. 2, which identifies four participants in the DR scheme, namely power system, TSO, IDC central controller interfaced with the power system control center, and energy management systems (EMS). System frequency and RoCoF are measured from each area of the power system by utilizing a number of phasor measurement units (PMU) sparse in the network. The PMU devices use a global positioning system (GPS) to transmit real-time snapshots of the frequency with small time-steps of 20 ms [38] via communication channels. These data are processed in the central controller enabling regulation signals ($R(t)$) for the IDC central controllers to provide FFR at time instant (t).

It is to be noted that from the system operator perspective, the faster IDC response is desirable to quickly offset frequency deviation at the early stage of the disturbance. Thus the current scheme of FFR service mandates delivery of the contracted resource magnitude within 2 s from the start of the disturbance while incentivizing quicker response times [14]. However, from the IDC perspective, controllable IT loads may not immediately respond due to the actuation delay as well as delay associated with the communication signals received at the IDC central controllers. Currently, a variety of communication techniques are deployed in wide-area monitoring systems such as fiber optic, telephone lines, satellite links, etc. each method has a certain delay that is in the range of 100 ms, 200 ms, and 500 ms respectively [39]. The significant impact of these delays on the dynamic performance of the system frequency response will be considered in Sub-Section 5.3.

3.1. System operator

The system operator is the licensed entity that continuously monitors demand and supply variations. The main task of the TSO is to pre-set a frequency defense plan against disturbance based on the availability of inertia and wind penetration level in the system. Here the TSO is assumed to receive regular information about the capability of IDC resources participating in the FFR service from the IDC central controller. Accordingly, the TSO runs an optimization process to prioritize the available resources in each area, considering constraints within the

system inertia, spinning reserve, and transmission line capabilities. This process does not need to be conducted in real-time and is only required when there is a significant change in the system status (i.e., level of wind power, and FFR resource availability) [38]. This is a stand-a-lone control system that is updated periodically during which the TSO requests required response latency e.g., ramp rate limit (dp/dt), MW volume of response power (ΔP_{FFR}), response time (T_R), and sustained time (T_{FFR}) from IDC central controllers.

3.2. Central controller

Data centers providing ancillary FFR services remain in normal operational condition until called upon during large disturbances to reduce their power consumption. Once the dispatch command $R(t)$ is received, based on the nature of the signal (e.g., regulation up or down $\in [P_{FFR}^{up}, P_{FFR}^{down}]$), the IDC central controller uses a number of local MPCs to assign reference signals (U_{UPSi}) and (U_{DRi}) to each resource participating in the FFR service to counteract a part of the estimated disturbance, as shown in Fig. 2. The controller computes control actions based on the state space predictions to prevent threshold violation of system frequency deviations while respecting IDCs resource level constraints. It is assumed that the central controller has full knowledge of the status and characteristics of IDC servers and UPS systems and can perform direct control actions in communication with the EMS. This assumption is considered for simplicity and transparency, and to set upper and lower constraints on IDC response capability.

The first control signal (U_{DRi}) minimizes the power consumption of the IDC servers at the most beneficial time, demonstrating suitable efficient predictions of the system needs for active power to arrest system frequency drop as quickly as possible. The second command signal will be issued to the UPS system (U_{UPSi}), the objective of which is to provide the fastest maximum power response in the event of frequency disturbances, thereby contributing additionally to the FFR service. The MPC method places reference active power order for the UPS in each delivery period to participate in the FFR service in which $\forall \Delta P_{UPSi}^M \in [P_{UPSi}^{min}, P_{UPSi}^{max}]$. When the FFR service is delivered, IDCs can transition all resources back to normal operation after T_{FFR} following the event initiation. This procedure is implemented in cooperation with the IDC EMS and named a low-level real-time control process due to the instantaneous response (i.e., $T_R < 2$ s).

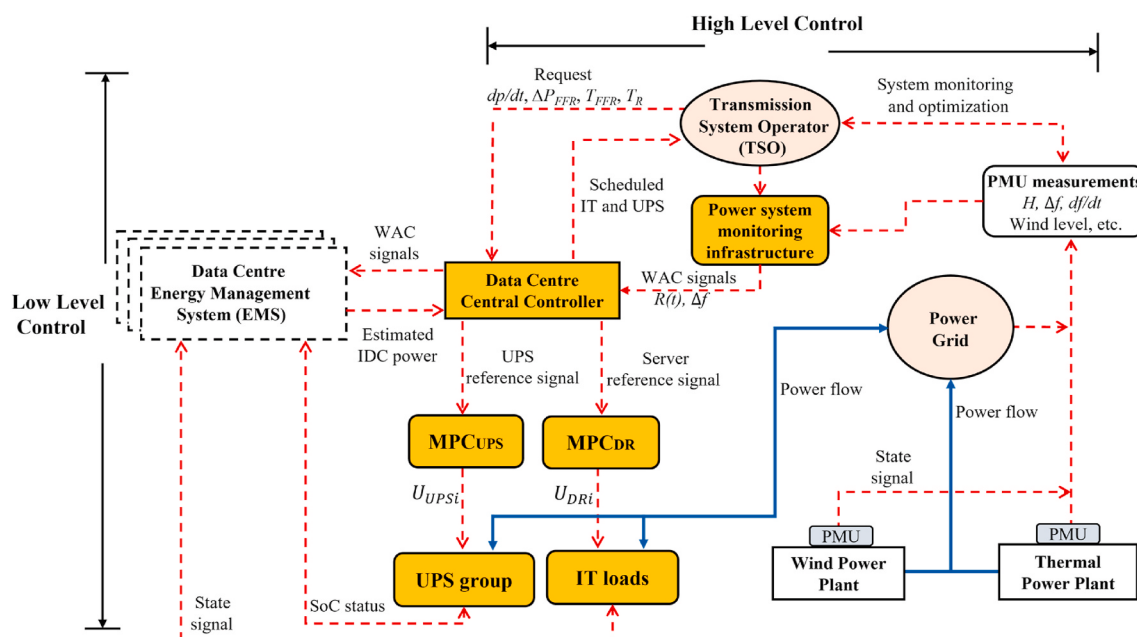


Fig. 2. Structure of the proposed centralized real-time FFR framework.

3.3. Data center energy management

The EMS responds autonomously to the central controller frequency deviation signals through optimal management of the IDC non-critical workloads (e.g., video streaming). Here it is assumed that EMS implements the first come first out (FIFO) policy for scheduling server jobs while respecting SLA. Based on the available and forecasted nonessential workloads, the EMS computes the aggregated power capacity (ΔP_{DR}) and drives a virtual droop curve (K_{DR}) for the server load power consumption. Similarly, the statistics of the UPS systems (i.e., available power (ΔP_{UPS}), and state of charge (SoC) levels) will be estimated to allocate enough storage capacity for the critical IT loads while respecting the FFR request signals. In this analysis, the steady-state SoC_{max} of the UPS is set to 80 % and no power exchange with the network during the load flow operation [40]. With this setting in place, there will be a 20 % tolerance to protect against transient over-frequency disturbances. Different from conventional energy storage, the SoC_{min} of the UPS system is set to deplete down to 40 % to prolong the UPS lifetime and to account for worse case scenarios if the power system completely crashed to recover from the frequency event.

4. Dynamic modeling of grid-scale IDC for frequency response analysis

4.1. Dynamic modeling of the power system under study

This subsection presents the dynamic model of the i th Area in a Three-Area simplified 39 Bus system. It is to be noted that the remaining two areas are identical except that IDC resources are only integrated into Area 1. As illustrated in Fig. 3, conventional power plants (CPP) are available to participate in load frequency control (LFC) and system balancing services during steady-state and transient events. The CPPs are equipped with a steam turbine, which includes both fast and slow power system dynamics. The variables (T_{gi} and T_{ti}) represent generator governor and turbine time constants, respectively, whereas β_i is the area bias factor, in which detailed parameters associated with the system can be established [18]. Furthermore, constraints and conditions required

by real power systems are also considered (e.g., generation rate constraint (GRC) is applied to the CPPs). The GRC of non-reheat thermal generation is set at 12 % p.u. MW/min to be consistent with the Irish grid code requirements for normal operating frequency variations [41].

Load frequency dependence is set to 1 p.u., to capture the essential characteristics of the load, and lumped into a damping constant (D_i) using the system base of 1000 MVA. Furthermore, an area control error (ACE_i) is applied with the help of a proportional-integral-derivative (PID) controller for the provisioning of the secondary frequency control loop. Under normal operation, the generator deadband (GDB) is specified as (0.03 %) to maintain system frequency deviations (Δf_i) within the nominal permissible range ($f_{DB, CPP} = \pm 15$ mHz) [41]. However, in the event of serious generation/demand imbalance, associated with the rapid frequency change, the primary frequency control of synchronous generators will be activated. These generators deploy droop coefficients (R_i), setting between 3 % and 5 % according to the Irish grid code for the provision of primary frequency response. Reserve from conventional resources is limited to 75 % of the largest single infeed (LSI) to be consistent with the traditionally required POR in Ireland and Northern Ireland power systems [42].

In this analysis, wind farms based on the doubly-fed induction generator (DFIG) wind turbine models are integrated into each control area and the detailed parameters associated with the wind generator are given in Ref. [43]. It is worth noting that the proposed DFIGs are not involved in the LFC and thus the output power variations are directly interfaced to the area controller. The variability in wind power is modeled using the standard deviation of wind speed multiplied by random output fluctuations which are implemented utilizing a white noise block along with a low-pass filter in Matlab/Simulink environment. A cubic function in (1) is used to determine output power generation from the wind speed data.

$$P_{wi} = 1 / 2 \cdot \rho \cdot A \cdot C_p(\lambda, \beta) \cdot V_w^3 \quad (1)$$

where ρ is the air density, A represents swept area, C_p indicates power coefficient, V_w is the wind speed, λ and β are tip speed ratio and pitch angle, respectively. Total wind power generation in the system is varied

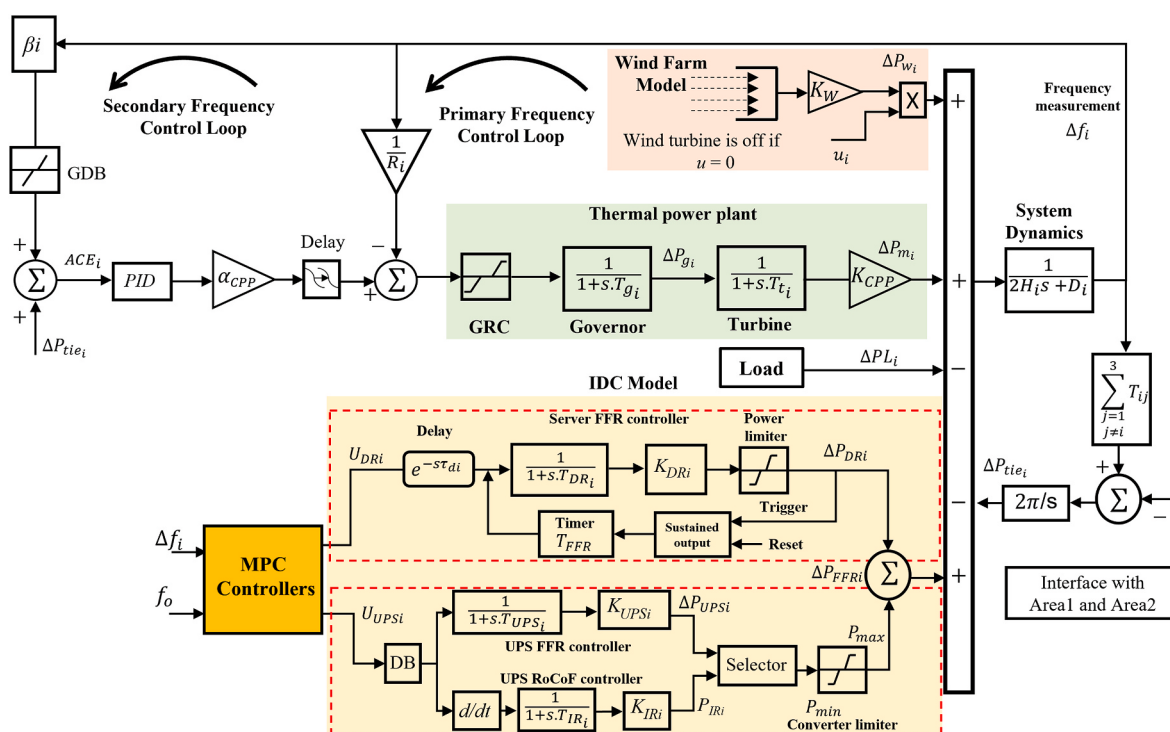


Fig. 3. The frequency response model of i th Area in a Three-Area power system with DFIG wind turbine and IDC dynamic models.

through four main operational dispatches in which the total system inertia and the POR of synchronous generators are systematically reduced, as summarized in Table 1. The TSO controls the power generation dispatch of synchronous generators and wind farms, in each area, using CPP distribution coefficient factors (K_{CPP}) and wind farm distribution coefficient factors (K_W) respectively. It is to be noted that the level of wind penetration, in this analysis, reflects the anticipated average wind generation in the Irish power system for 2030 [2]. Under no wind operational dispatch, the total inertia of the system is expected to be about 2410 MW s which corresponds to $H = 2.41$ s on the system base. This value is scaled up to be in line with the current operational constraint limit that ensures the all-island inertia does not fall below 23,000 MW s [42]. However, in Ireland, the operational limits for the system inertia floor are likely to be reduced while deploying a new RoCoF limit of 1 Hz/s in 2030 [7]. Thus we run extensive dynamic analysis to show the capability of IDCs to facilitate the requisite reduction in the minimum synchronous inertia level and securely operate at 75 % SNSP (see Table 2).

Furthermore, IDC UPS and IT loads are the last two essential elements in the area controller, with the model parameters found in Refs. [17,44], respectively. The UPS and DR units, in this analysis, employ a generalized low-order model that holistically presents the flexibility constraints of each resource. Although higher-order dynamic models can be deployed for the UPS and DR units, the low-order dynamic models considered in this analysis are sufficient to evaluate frequency control over a short transient time window of 30 s [17,18], and [44]. The control design for each of these elements and the algorithm related to their operation are described in Sections 4.2 and 4.3. To ensure the system robustness and practicality, communication and actuation delay time issues with the FFR service have also been fully considered in the system design using a time delay ($T_d = e^{-s\tau_{dt}}$) block expressed in the Laplace domain. The time delay of the control loop is calculated using (2).

$$\tau_{di} = \tau_{ci} + \tau_{ai} \quad (2)$$

where τ_{ci} presents the communication delay in (s), τ_{ai} is the server actuation delay which is set to 6 ms [31,32]. It is to be noted that one of the essential properties of a power system dynamic is related to continuous electromechanical oscillations. If delays are increased at the input of the controller, the IDCs will begin to inject active power into the network quickly in anti-phase with the electromechanical energy of synchronous generators. As the system dynamics become fast at high wind penetrations, delays can push the action of the controller closer to 180° out of phase with the system electromechanical dynamics. Indeed, this is extremely dangerous as it results in frequency overshoot and at high SNSP levels, it may drive the system to complete instability. Theoretically, the delay time (τ_d) introduces phase lag (ϕ) in the input signal of the controller for an oscillation mode with frequency (f) [45]. The magnitude of the phase lag can be determined mathematically using (3).

$$\phi_i = 360^\circ f \tau_{di} \quad (3)$$

As an example, a delay time of 100 ms in a communication channel for a dominant frequency of 0.5 Hz can bring in a phase lag of $360^\circ \times 0.5 \times 0.1 = 18^\circ$. Equation (3) indicates that ϕ is affected by both the τ_d and oscillation mode f . For the same f , the corresponding phase lag is

Table 1
System configurations for different operational power dispatches.

Operational dispatches	Wind penetration	System inertia (H) (s . p.u)	CPP distribution coefficient (K_{CPP})	Wind farms distribution coefficient (K_W)	Reserve per area (p.u)
No wind high inertia (NWHI)	0 %	2.41	1 p.u.	0	0.375
Low wind high inertia (LWHI)	40 %	1.446	0.6 p.u.	0.4 p.u.	0.375
Medium wind medium inertia (MWMI)	60 %	0.964	0.4 p.u.	0.6 p.u.	0.375
High wind low inertia (HWLI)	75 %	0.602	0.25 p.u.	0.75 p.u.	0.375

Table 2
Data center resource parameters.

Parameters	UPS	IT loads
ΔP_{FFR}	250 MW	100 MW
Power/unit	1 MW	0.335 kW
Number of units (M)	500	1,755,926
Gain (K)	$K_{IR} = 3, K_{UPS} = 2$	$K_{DR} = 1$
$dP^{(\pm)}/dt$ [MW/s]	500	200
T_R [s]	$0.2 \geq$	$0.25 \geq$
T_d [ms]	100	200
T_{FFR} [s]	60	90
$f_{DB,FFR}$ [mHz]	20	20

larger with higher delay signals. Thus generating a phase lead will be an essential need in order to compensate for the impact of phase differences and neutralize the impact of communication delays. Indeed, a number of methods have been developed to approach this issue including delay compensators with fixed parameters [46]. Nevertheless, time delay compensators are more sensitive to process parameter settings which requires self-tuning in complex applications. This has been managed in Refs. [47,48] using an adaptive delay compensator, which is out of the scope of this paper.

Now system frequency dynamics of a center of inertia (COI) of the complete one area system can be derived from the swing equation using (4) and (5). Here the whole system generators in the area are modeled as an equivalent synchronous machine. Such a representation is practically proven to be sufficiently accurate for dynamic frequency stability [18, 44], and [49].

$$2H_i \frac{d\Delta f_i}{dt} + D_i \Delta f_i = \Delta P_{mi} - \Delta P_{Li} \quad (4)$$

Traditionally, the primary and secondary frequency control loops were responsible for restoring system frequency deviation following a sudden power imbalance in the system. However, the POR is not fast enough at high wind power generation. Thus, the combined FFR service and POR are essential to arrest and recover the frequency to the nominal value using (5). It is obvious that the FFR based on the IDC control loop gives more freedom to the TSO to keep the frequency deviation within the permissible range.

$$\dot{\Delta f}_i = -\frac{D_i}{2H_i} \Delta f_i + \frac{1}{2H_i} \left[\sum_{k=i+1}^{N,M} (\Delta P_{mi}^k \cdot K_{CPP} + \Delta P_{wi}^k \cdot K_W) - \sum_{k=i+1}^{N,M} (\Delta P_{Li}^k + \Delta P_{tie,i}^k) + T_d \sum_{k=i+1}^{N,M} \Delta P_{FFR,i}^k \right] \quad (5)$$

where Δf_i is the frequency deviation due to a disturbance in (Hz). H_i and D_i denote the equivalent inertia constant and damping coefficient in the Area, respectively. As an example, if the value of D_i is set to 1, it means that a 1 % change in the system frequency would result in 1 % of load variations [18]. N is the set of control areas which is three in this analysis. ΔP_{mi} and ΔP_{Li} are the total power generation and demand. ΔP_{wi} presents uncertainty associated with the output power generation of the integrated wind farm area i . $\Delta P_{FFR,i}$ is the aggregated IDCs response power. M is the number of participated units. $\Delta P_{tie,i}$ tie-line power flow between two adjacent areas can be expressed in (6). From the point of

view of power balance, the ΔP_{tie} can be added to the ΔP_L of the area.

$$\Delta \dot{P}_{tie_i} = 2\pi \sum_{j \in N-(i)}^N T_{ij} (\Delta f_i - \Delta f_j) \quad (6)$$

where Δf_i and T_{ij} are the frequency deviation and synchronizing torque coefficient of a transmission line between two adjacent areas i and j , and N is the total number of areas.

4.2. FFR resource modeling

4.2.1. Data center resource coordination

The dynamic power exchange between the IDC components and the power system is modeled using first-order transfer functions to present holistically the flexibility and constraints of two types of controllable operating resources (e.g., UPS and IT loads). Each IDC UPS system may be featured to provide a combination of very fast responding virtual IR (P_{IRi}) and fast frequency response (P_{FFRi}). The former is usually instant initiation with a response time (e.g., $T_R \leq 300$ ms) when Δf_i is outside the frequency deadband ($f_{DB,FFR} = 20$ mHz), while the latter is a relatively slower response (e.g., $T_R \leq 2$ s) and larger energy rating [14]. These signals are weighted by (K_{IRi}), (K_{UPSi}) and (K_{DRi}) factors to present the IR and FFR gains, respectively. The response from the UPS and IT loads are coordinated to perform actions considering the characteristics and capabilities of each resource so that the net response is quick and sustained for a sufficient timescale to handover with the POR and secondary operating reserve (SOR) services [42]. It is to be noted that a number of parameters are used to coordinate each resource participating in the FFR (e.g., T_R , dp/dt , ΔP_{UPS} , ΔP_{DR} , and T_{FFR}) [38]. This is graphically illustrated for an under-frequency event using the ideal active power-frequency curve in Fig. 4. It is noteworthy, that the response to an over-frequency disturbance will follow the same pattern. As can be seen, compared to the synchronous generators, a larger deadband is chosen for the FFR service in order to accounts for uncertainties associated with wind power variability.

The UPS frequency controller is synthesized by two lag blocks that can be added to the power converter to dispatch active power based on the swing equation. The inertia response controller is computed based on the RoCoF to add extra active power when a disturbance appears. As the RoCoF controller is hypersensitive to noise, a low-pass filter is integrated into the control loop, as in (7):

$$P_{IRi} = \frac{K_{IRi}}{1 + sT_{IRi}} \left(\frac{df}{dt} \right) \quad (7)$$

where s denotes Laplace operator, $f_o \in R$ is the nominal system frequency in (Hz), df/dt is the rate of change of frequency (RoCoF) in (Hz/s), $P_{IRi} \in R$ is the delivered emulated power in (MW), and T_{IRi} is the UPS RoCoF

controller time constant in (p.u). Considering that the response time of IR of all UPS units is considerably the same across the ISC [16], the IR power injected can be approximated using (8).

$$P_{IRi} \approx K_{IRi} \left(\frac{df}{dt} \right) \quad (8)$$

For the purpose of this analysis, the UPS units are equipped with the selector block that enables the controller to switch between IR and FFR based droop characteristic services when required. The overall delivered power (ΔP_{UPSi}) can be presented as in (9).

$$\Delta P_{UPSi} = \left[\Delta f_i \frac{K_{UPSi}}{sT_{UPSi} + 1} + K_{IRi} \left(\frac{df}{dt} \right) \right] U_{UPSi} \quad (9)$$

where T_{UPSi} represents the UPS FFR controller time constant. As we have implemented an aggregator containing six IDCs, the T_{UPSi} values are varied between 5 and 7.5 p.u in step 0.5. $U_{UPSi} \in R$ represents a control signal received from the IDC MPC controller. For proportional sharing of the IR among all participating UPS units during disturbances, it is implicit that $K_{IRi1} = K_{IRi2} = \dots K_{IRin} = K_{IR}$, where $K_{IR} \in R \geq 0$ is the coordinated IR gain among all UPS systems. Similarly, the droop coefficients for all UPS controllers are coordinated through the controller gains to specify the rate of change of the UPS power (dp/dt) so that $K_{UPSi1} = K_{UPSi2} = \dots K_{UPSn} = K_{UPS}$. Where $K_{UPS} \in R \geq 0$ represents the coordinated FFR gain among all participants. In a typical IDC, there might be more than one UPS system that is willing to participate in the FFR service. The mean power reference for the i th UPS in the IDC ($\Delta P_{ref}^{UPSi} \in R$) can be calculated by a simple proportional algorithm:

$$P_{ref}^{UPSi} = \alpha_i P_{ref}^{UPSiDC} \quad , \quad \text{with } \alpha = \sum_{i=1}^M \alpha_i = 1$$

where M is the number of UPS systems in the IDC, P_{ref}^{UPSiDC} is the power reference for the total quantity of UPS systems participating in the FFR service, α_i is the sharing factor for the i th UPS system. Lastly, the FFR of the IDC servers is presented by another transfer function as in (10).

$$\Delta P_{DRi} = \left[\frac{K_{DRi}}{1 + sT_{DRi}} \right] U_{DRi} \quad (10)$$

where T_{DRi} is the time constant of the IT load FFR controller and for simplicity, it is assumed that all servers in a particular IDC have the same time constants varied between 0.3 p.u and 0.4 p.u, $K_{DRi1} = K_{DRi2} = \dots K_{DRin} = K_{DR}$ for $K_{DRi} \in R \geq 0$ is the controller gain utilized for proportional sharing between one IDC to another. The controller gain can also specify the rate at which IT load power consumption (dp/dt) changes. $U_{DRi} \in R$ is the controller reference signal. Due to the fact that the UPS systems are coordinated by a droop frequency controller, the EMS in an

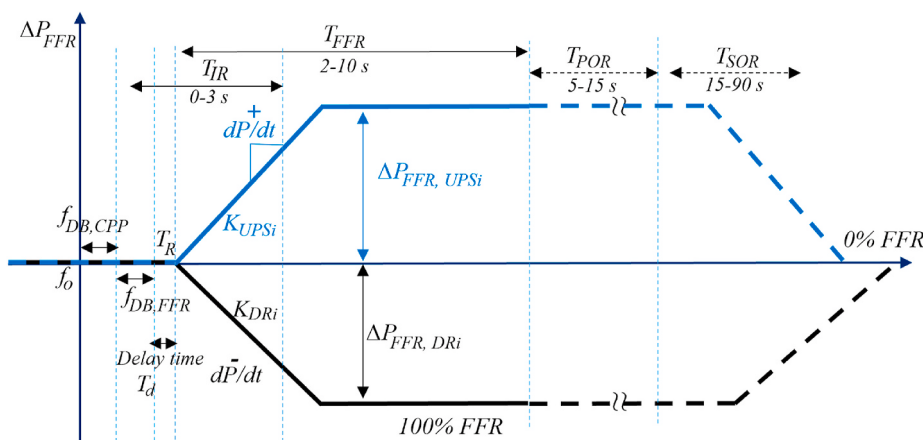


Fig. 4. Proposed active power-frequency response for coordinating UPS systems and IT workloads.

IDC needs to manage a group of IT loads as virtual energy storage with a virtual droop curve [49]. Thus, based on the available maximum and minimum delay-tolerant loads $\forall \Delta P_{DR_i}^M \in [P_{DR_i}^{min}, P_{DR_i}^{max}]$, the corresponding droop curve can be derived, as shown in Fig. 4. Whereby the response is sustained while the frequency recovers to quasi steady-state similar to response required from PV power plants in Australia [50]. Practically, response duration (T_{FFR}) depends on the sensitivity of delay-tolerant workloads. Now the total power dispatched ($\Delta P_{FFR_i} \in R$) by the i th IDC can be formulated using (11).

$$\Delta P_{FFR_i} = \sum_{i=1}^M \Delta P_{UPSi} + \Delta P_{DR_i} \quad M \in R \quad (11)$$

4.2.2. Data center resource availability

This subsection illustrates the excess energy availability in data centers using the high demand forecast scenario for IDCs in Ireland in 2028, as explained in Section 1. Joint participation of 350 MW of IT servers and UPS systems for the provision of FFR service is investigated. This surplus energy is a result of IT workload shifting and UPS redundancy, respectively. The analysis is based on the fact that IT loads have a typical power consumption of 50 % of total data center energy usage [21]. It was assumed that each IT server has a typical power consumption of 0.335 kW [32]. The maximum regulation capacity of the IT servers is set to 17 % of its nominal power consumptions [31,32]. Thus, using the high demand forecast scenario, it is estimated that IT servers could participate in DR programs with up to 170 MW for both regulations up and down.

Furthermore, for the provision of FFR service, the UPS systems are only needed for a short period of 10 s after the frequency change, meaning they do not require a huge storage capacity. However, they can also remain in operation to participate in other ancillary services (e.g., POR and SOR services). In this analysis, each UPS device is presumed to be equipped with battery capacity for 10 min of autonomy time. This is a typical design value in data centers and similar to Ref. [25] is supposed to correspond to 167 kWh of energy, meaning 1 MW/UPS for a window of 10 min. However, the expected power requirement to securely operate critical loads in each IDC during this timeframe is set to 500 kWh which corresponds to 3 MW for 10 min. Using the 2 N topology UPS redundancy, the total accumulated and total exceeded bi-directional energy in the UPS will be 1000 kWh and 500 kWh respectively. With this configuration, there will be three UPS systems each with a 1 MW dispatch capacity that can be used to inject or absorb power from the network during disturbances. Nevertheless, in this analysis, the maximum capabilities of both the IT loads and the UPS are constrained to 100 MW and 250 MW in each scenario, respectively, using the MPC method. Furthermore, the maximum dispatch durations for both resources are limited to the end of SOR service in Ireland and set at 60 s and 90 s correspondingly [42]. This is to avoid second frequency dip which may appear during the charging process of the UPS. The detailed implemented parameters for the proposed IDCs are given in Table 2.

4.3. MPC based fast frequency response for data centers

4.3.1. State-space formulation

In this subsection, the linearized state-space model of a power system with integrated IDCs is deduced from (5), (6), (9), and (10). These equations represent the complete state-space model of the linear time-invariant power system described in Fig. 3 in sub-section 4.1. The dynamic model of the IDC and wind farms are also formulated.

$$\begin{cases} \dot{x}_i(t) = A_i x_i(t) + B_i u_i(t) + E_i d_i(t) \\ y_i(t) = C_i x_i(t) + D_i u_i(t) \end{cases} \quad (12)$$

$$x_i = [\Delta f_i \quad \Delta P_{ie,i} \quad \Delta P_{UPSi} \dots \Delta P_{UPS,M_i} \quad \Delta P_{DRi} \dots \Delta P_{DR,M_i}]^T \quad (13)$$

where $x_i \in R^2$, define the state vector at discrete time step k and $u_i \in R^{N+1}$

denoting a control vector for the IDC resources, $y_i(t) = \Delta f_i$ is the output vector, A_i , B_i , C_i , D_i and d_i are the system matrices and d_i is the disturbance vector. As (12) implies the uncertainty associated with the wind power fluctuation is included as a measured disturbance in the state space equations. The power system state and input and output matrices can be expressed as:

$$A_i = \begin{bmatrix} \frac{-D_i}{2H_i} & -1 & \frac{1}{2H_i} & \dots & \frac{1}{2H_i} & \frac{1}{2H_i} & \dots & \frac{1}{2H_i} \\ P_{tieij} & 0 & 0 & \dots & 0 & 0 & \dots & 0 \\ 0 & 0 & \frac{1}{T_{UPSi,i}} & \dots & 0 & 0 & \dots & 0 \\ \vdots & \vdots & \ddots & & & & & \\ 0 & 0 & 0 & \dots & 0 & \frac{1}{T_{UPSMi}} & 0 & \dots & 0 \\ 0 & 0 & 0 & \dots & 0 & \frac{-1}{T_{DRi}} & \dots & 0 \\ \vdots & \vdots & \ddots & & & & & \\ 0 & 0 & 0 & \dots & 0 & 0 & \dots & \frac{-1}{T_{DRMi}} \end{bmatrix}$$

$$B_i = \begin{bmatrix} 0 & 0 \\ 0 & 0 \\ K_{UPSi} & 0 \\ \vdots & K_{DRi} \\ K_{UPSMi} & \vdots \\ 0 & K_{DRMi} \end{bmatrix}, \quad C_i = \begin{bmatrix} 1 \\ 0 \\ 0 \\ \vdots \\ 0 \end{bmatrix}^T, \quad E_i = \begin{bmatrix} \frac{1}{2H_i} & \frac{-1}{2H_i} \\ 0 & 0 \\ 0 & 0 \\ \vdots & \vdots \\ 0 & 0 \end{bmatrix}, \quad D_i = 0 \quad (14)$$

$$d_i = [\Delta P_{wi} \quad \Delta P_{Li}]^T \quad u_i = [U_{UPSi} \quad U_{DRi}]^T \quad (15)$$

where $P_{tieij} = \frac{2\pi}{s} \sum_{j \in N-(i)} T_{ij}$, N is the set of controlled areas, u_i includes the control variables for the UPS and DR reference signals (U_{UPSi}) and (U_{DRi}), respectively. In this study, uncertainties associated with wind power variations (ΔP_{wi}) and load power changes (ΔP_{Li}) are considered as disturbance signals.

4.3.2. Objective function and constraint formulation

The MPC method implies state measurements to generate reference signals (U_{UPSi} and U_{DRi}) for each IDC while optimizing an appropriate cost function, as depicted in Fig. 5. The controller combines an optimization mechanism with the system constraints and limitations throughout a finite time horizon. Assuming that $H = \{k, k+1, \dots, k+N\}$ denotes the MPC prediction horizon over N_p , and k is the current controller time step. As the main interest of this study is in the dynamics of the network (5) subject to a sudden power imbalance, the proposed optimization problem aims at minimizing frequency nadir to prevent critical threshold violations (e.g., $50.5 \geq \Delta f \geq 49.5$ Hz) while respecting IDC resource constraints. This is the maximum permissible steady-state frequency deviation after 1 s following a disturbance [14]. The second objective of the optimizer is to minimize the control efforts ($u_i(k)$) over the full prediction horizon N_p (i.e., $\forall k \in H$) while ensures sufficient IDC reserve is available to meet the loss of LSI. It is essential to integrate this information into the power system economic dispatch [51,52] in order to guarantee the predicted Δf following the loss of the largest generator for a given operational dispatch stays above the security threshold limits ± 0.5 Hz.

The proposed controller utilizes the MPC active set solver, that implements the Knows What it Knows (KWIK) algorithm [17] to periodically solve the following quadratic programming problem at each step of the optimization:

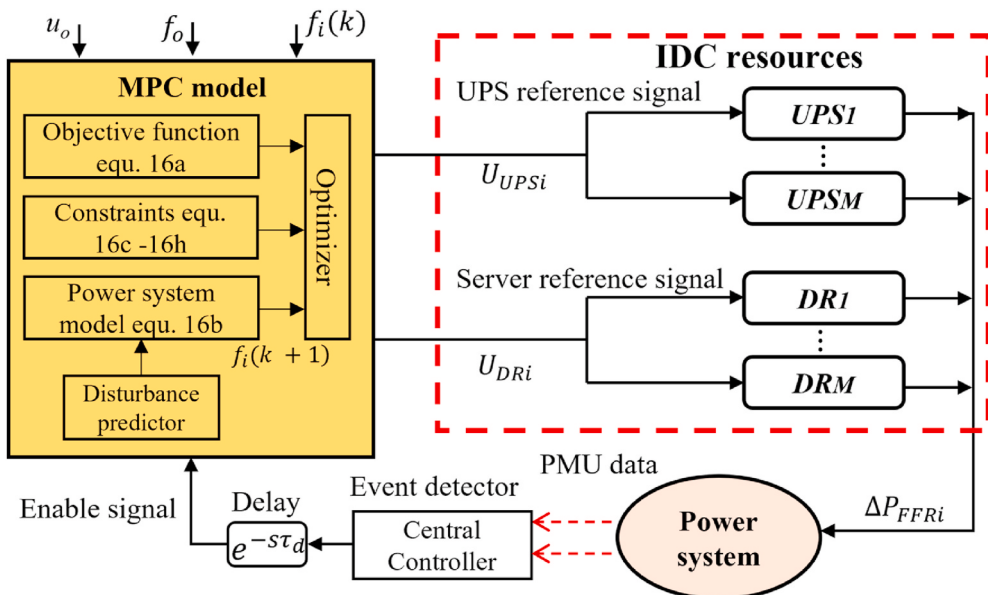


Fig. 5. Schematic diagram of the deployed MPC method to control IDC resources.

$$\begin{aligned}
 J(k) = & \underbrace{\sum_{i=0}^{N_p} \{f_i(k+i|k) - f_o(k+i|k)\}_{Q_f}^2}_{\text{Term 1}} + \underbrace{\sum_{i=0}^{N_c-1} \{ \Delta u_{UPSi}(k+i|k) \}_{Q_{UPSi}}^2}_{\text{Term 2}} \\
 & + \underbrace{\sum_{i=0}^{N_c-1} \{ \Delta u_{DRi}(k+i|k) \}_{Q_{DRi}}^2}_{\text{Term 3}}
 \end{aligned} \quad (16a)$$

s.t.

$$x_i(k+1) = A_i x_i(k) + B_i u_i(k) + E_i d_i(k)$$

$$\Delta f_{max} \leq \Delta f_i \leq \Delta f_{min}$$

$$u_{UPSimax} \leq u_{UPSi} \leq u_{UPSimin}$$

$$u_{DRImax} \leq u_{DRi} \leq u_{DRImin}$$

$$P_{UPS}^{min} \leq \Delta P_{UPSi} \leq P_{UPS}^{max}$$

$$P_{UPS}^{max} \leq \max_{t \geq T_R} P_{UPS}(t) \quad \forall t \in T_{FFR}$$

$$SoC_{UPS}^{min} \leq SoC_{UPSi} \leq SoC_{UPS}^{max}$$

$$E_{UPS}^{us} = (SoC_{max} - SoC_{min}) E_{UPS}^a$$

$$E_{UPS}^{max} \leq \max_{t \geq T_R} E_{UPS}(t) \quad \forall t \in T_{FFR}$$

$$P_{DR}^{min} \leq \Delta P_{DRi} \leq P_{DR}^{max}$$

$$P_{DR}^{max} \leq \max_{t \geq T_R} P_{DR}(t) \quad \forall t \in T_{FFR}$$

where $f(k+i|k)$ is the predicted output at sampling instant k . $\Delta u(k+i|k) = u(k+1) - u(k+i-1)$ is the predicted reference signal increment. N_p and $N_c \in R > 0$ are the predicted and the control horizons respectively, their values are defined in [Table 3](#). The controller predicts the operational states of the shifted workload as well as the SoC of the UPS over a window of 2 s, the time that mandates the FFR service to reach full active power. When the control horizon N_c ($N_c \leq N_p$), the quadratic performance index of the optimization function satisfies [\(16a\)](#). For a plant containing delays, it is good practice to specify $N_p - N_c \gg \tau_d$. *Sampling time*. With this setting, the controller will have a complete

Table 3
MPC method parameter definitions.

Parameters	Values	Parameters	Values
Q_f	0.51	f_0	50 Hz
Q_{UPS}	0.73	u_o	0
Q_{DR}	0.82	N_p	20
Sample time	0.1 s	N_c	3

image of the decision variable on the future states in the presence of delays. Nevertheless, this setting does not necessarily guarantee long time delays as well as stochastic delays which may require complex optimization algorithms. Q_f , Q_{UPS} , and $Q_{DR} \in R \geq 0$ are the weighting matrices that compromise the output error and control effort. Sensitivity analysis is used to verify the best weights for the controller such that it incentivizes the use of control resources at an earlier time step to avoid late reactions as well as frequency oscillations near the frequency limit resulting from the resource reference signal variations. Small weight values mean that the corresponding variable has less impact on the overall performance index. In this analysis, the larger weight factor is set on the IDC servers as it is assumed to be able to delay workloads and sustain for a longer time duration.

The first term of the cost function is associated with the error in system output over the prediction horizon that minimizes the frequency deviation metric (Δf_i) with respect to the reference signal $f(k+i|k)$. The second and the third terms indicate control efforts over the horizon N_c that minimize reference signal variations for the UPS and DR units, respectively. At the current discrete sampling period $k \in Z \geq 0$, the controller receives the latest available measurements from the data center central controller and utilizes state space-based predictions to estimate the optimal control sequence $u(k), u(k+1), \dots, u(k+N_p-1)$ over a horizon of $N_p \in Z \geq 0$ future sampling time steps to satisfy the applied constraints at the minimum cost. Typically, the first control sequence $u(k+1)$ is implemented as the actual control signals for the UPS and DR units, and the rest of the sequences are discarded.

Moreover, constraints [\(16b\)](#) and [\(16c\)](#) ensure the security of the power system remain within the permissible range (i.e., $\Delta f = \pm 0.5$ Hz) while [\(16d\)](#) and [\(16e\)](#) are constraints on the MPC output reference signals to control the injected power during each sampling instant (k). Physical limitations for each resource are also considered using constraints [\(16f\)](#) – [\(16l\)](#). These include the upper and lower bounds of the

aggregated power from deferable server jobs as well as the UPS converter limitations. Equation (16h) guarantees the SoC of the UPS batteries does not surpass the predefined values. As the storage cost is significantly affected by the maximum installed capacity and the rate of energy delivered, these metrics are carefully constrained as follow:

- Maximum installed capacity (P_{UPS}^{max}): constraint (16g) ensures the UPS does not exceed its maximum installed capacity at any time during the FFR timeframe (T_{FFR}). This metric is practically essential in order to correctly size the converters (i.e., a larger value of P_{UPS}^{max} meaning a larger converter will be needed).
- UPS energy rating: constraints (16i) and (16j) maintain the maximum useable energy (E_{UPS}^{us}) during the whole period of the disturbance within the total available energy (E_{UPS}^a) at any time (t). The maximum amount of energy supply determines the requisite storage capacity that highly contributes toward the overall storage cost.

Similarly, the remaining constraints (16k) and (16l) are applied to limit the maximum deferred power consumption of the IDC loads.

4.3.3. Disturbance predictor

A disturbance predictor is an essential part of the MPC method which is used to continuously predict the disturbance magnitude over the prediction horizon. This can significantly affect how far the controller can forecast future disturbances and how precisely the controller can select the control variables. Nevertheless, this research aims for the FFR service such that the prediction is going to be over a very short time period. Thus, for the purpose of simplicity and practicality of the model, a straightforward approach has been employed to predict frequency deviation in swing equation (4) during which the predicated disturbance power $P_d(k+1)$ is assumed to be equal to the current measured disturbance power $P_d(k)$. This assumption is in agreement with the previously

utilized MPC method for IR and FFR applied to grid-friendly distributed energy resources and wind farms in Refs. [15,16] respectively.

5. Results and discussions

The proposed IDC models with their control loop parameters have been implemented in MATLAB/SIMULINK platform. The dynamic performance of the system IDC frameworks is evaluated inside a simplified model representing the governor, inertia, and damping of the well-known standard 39 Bus New England system, as depicted in Fig. 6. As shown, the New England system is divided into three control areas with relevant loads, generators, and network data which can be found in Ref. [18]. The generalized LFC of one area of the system is described in Fig. 3 in Section 4.1. The New England grid is augmented with six geographically distributed energy-intensive IDCs integrated into Area 1. For simplicity, it is assumed that all IDCs in the area are owned by two ISC that provide internet-scale services with low latency and high reliability. The two ISCs share the same parameters, each of which participates in the IR and FFR services with a number of UPS and DR units, as described in Section 4.2.

Three operational scenarios are presented to evaluate the potential resilience benefits from the proposed IDC framework. Scenario 1 illustrates the capability of FFR from IDC resources to facilitate secure transactions to high wind power generation. The impact of different IDC resource configurations on the system frequency nadir, time to nadir, RoCoF, and tie-line stabilities under credible disturbances are extensively discussed. In Scenario 2, the importance of various IDC resources following non-credible cascaded system failure that may trigger UFLS protection relays are explored in the presence of wind power uncertainties. Lastly, the effect of communication and actuation latencies, that may appear during the response of IT servers, on the system frequency dynamics are examined in Scenario 3.

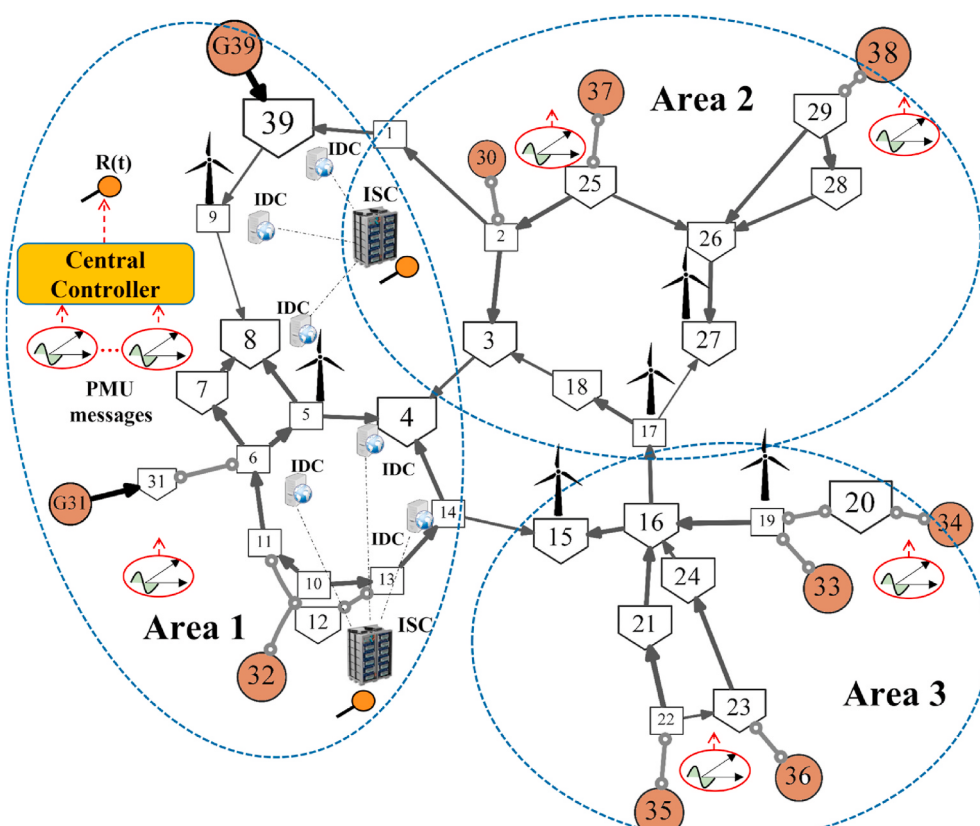


Fig. 6. The modified IEEE 39 bus system including data centers ISC, central controller, and wind farms.

5.1. IDC benefits in low-inertia systems

Dynamic performance of the power system with IDCs as a source of IR and FFR service is investigated using six case studies. For each case study, the disturbance is generated through a step change in active power with a value of 500 MW in Area 1 at 0 s and the test conditions are recorded for 30 s. This contingency reflects the outage of one of Ireland's LSI machines or current HVDC interconnectors with Great Britain.

- Case A: No IDC support
- Case B: UPS as a source of FFR service
- Case C: UPS joint with sustained IT loads as a source of FFR service
- Case D: UPS as a source of inertia response (IR)
- Case E: UPS as a source of inertia and FFR service (FFR-IR)
- Case F: UPS as a source of inertia and FFR service (FFR-IR) joint with sustained IT loads

5.1.1. Effect of IDC on the frequency response

The impact of wind penetration on the dynamic frequency response can clearly be seen from Case Study A in Fig. 7. As shown, the system frequency nadir as well as the quasi-steady-state frequency dropped significantly with the increased penetration of wind power generation. As an example, in dispatch NWHI, system frequency dropped to 49.59 Hz as a nadir, whereas for the same disturbance in dispatch HWLI, the frequency reached a nadir 48.81 Hz due to low inertia conditions. Indeed, in the Irish power system, such frequency decline could eventually breach both the Short Term Active Response (STAR) relay and the UFLS limits that automatically disconnects voluntarily contracted customers on the distribution network for the frequency deviations below 49.3 Hz and 48.85 Hz, respectively [41]. These results demonstrate that the capability of the active frequency response of synchronous generators becomes insufficient when the system is operated with high wind power generation that does not provide POR service. Thus additional under frequency containment supports are required to securely operate the system at 75 % wind penetration. This is where IDCs equipped with

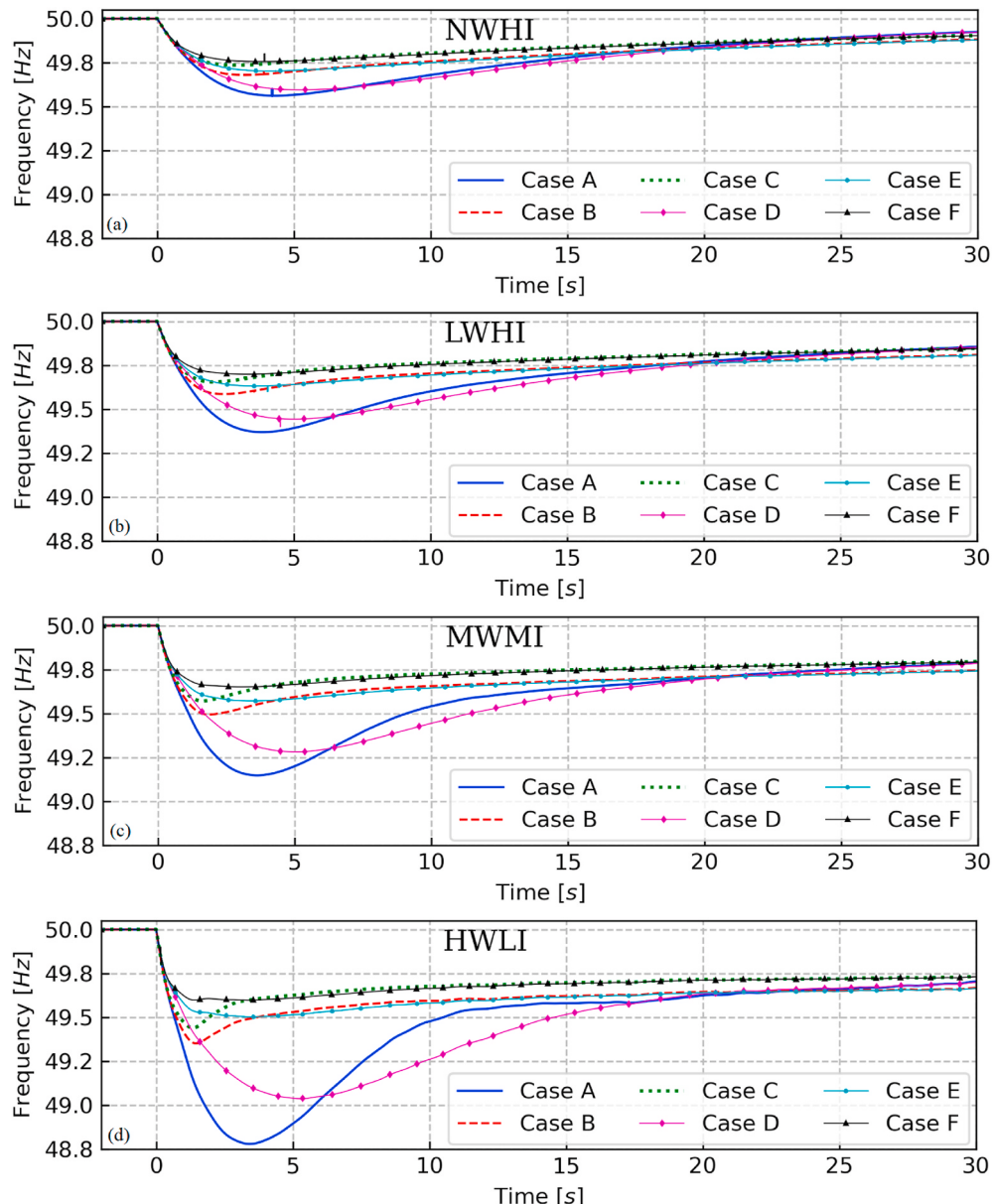


Fig. 7. System frequency response for different wind penetration levels (a) no wind high inertia (NWHI), (b) low wind high inertia (LWHI), (c) medium wind medium inertia (MWMI), and (d) high wind low inertia (HWLI).

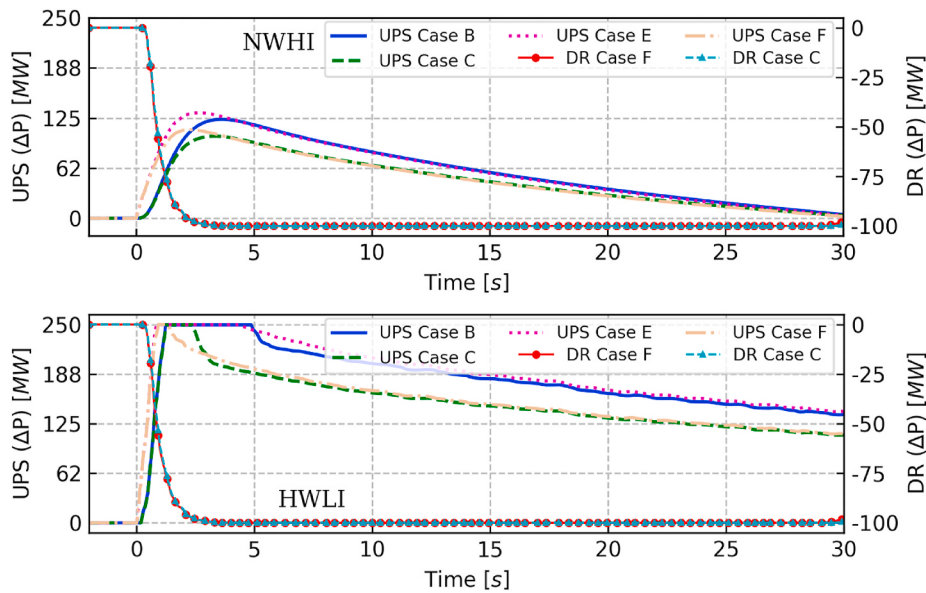


Fig. 8. Aggregated power injection from the UPS and DR units in response to the transient event for the low and high wind power dispatches.

frequency sensitive modes can play an essential role.

The impact of the proposed FFR method on the system frequency dynamics for the population of 350 MW IDC resources is compared in Fig. 7. Case Study B is conducted to examine the capability of the aggregated UPS systems to participate in the FFR service. Nevertheless, the impact of joint operation of 250 MW UPS system and sustained 100 MW IT loads on the frequency deviation is shown in Case Study C. Frequency responses for the same wind operational dispatches are recorded.

It is obvious that IDC UPS systems can arrest system frequency nadir above the tolerable limit for up to MWMI dispatch during which system frequency is arrested at 49.5 Hz. However, as demonstrated in dispatch HWLI, the aggregated IDC UPS supports failed to fully compensate the disturbance and thus the frequency is contained at a minimum point of 49.35 Hz. This has resulted from the constraints that the controller applies to the converter maximum power dispatch. It is essential to note that the addition of another 100 MW IT loads in coordination with the UPS units was able to enhance system frequency over the timeframe of the FFR and POR services. Clearly, the frequency deviation is arrested at 49.43 Hz as a nadir which is marginally higher than Case B but it is still below the tolerable limits. Similarly, the post nadir frequency reaches a quasi-steady state at 49.75 Hz which is lower than the NWHI dispatch which settles at 49.9 Hz. Generally, the steady-state frequency is higher in the case when joint support is provided from the UPS and DR units. This is because of the capability of IT loads to reduce their power consumption and sustain for the complete duration of the POR in contrast to the UPS units that exactly follow the system frequency trace.

The analysis is further developed to examine the impact of IR service on the system frequency performance. With this feature in place, the UPS can provide higher energy at the beginning of the disturbance in response to the system RoCoF. Shown in Fig. 7, system frequency traces for the three new case studies (D, E, and F) at different wind penetration levels. As illustrated, IR based UPS controller can considerably extend the time window of frequency deviation. It is worth noting that with an increasing level of wind penetration, the potential impact of virtual IR on the system frequency nadir increases. This clearly indicates that at high wind power generation, the system is highly dependent on the proposed IDC units to support system frequency.

A summary of the main indicators (i.e., nadir and time to nadir) used to assess the frequency response in each case study is provided in Table 4. It can be observed that severe and fast nadir is reached at high wind generation when the level of system inertia is extremely low. As an

Table 4

Summary of the main indicators used to assess frequency response for all dispatches.

Parameters	Case study	NWHI	LWHI	MWMI	HWLI
Frequency nadir [Hz]	A	49.56	49.36	49.14	48.81
	B	49.67	49.58	49.49	49.35
	C	49.73	49.65	49.57	49.43
	D	49.59	49.4	49.28	49.03
	E	49.7	49.6	49.57	49.5
	F	49.75	49.69	49.65	49.59
Time to Nadir [s]	A	4.3	3.85	3.63	3.13
	B	3.19	2.45	1.87	1.46
	C	2.86	2.04	1.65	1.34
	D	5.23	5.11	5.04	4.9
	E	4.04	3.62	3.47	3.43
	F	3.77	3.27	3.07	3.0

illustration, in dispatch NWHI Case A, system frequency reaches a nadir of 49.56 Hz after 4.3 s from the start of the event. However, for the same case in dispatch HWLI, the nadir of 48.81 Hz is reached after 3.13 s. This is an extremely short time for the remaining synchronous generator to activate the POR. Consequently, it takes less time for post-contingency frequency to move outside the permissible operating range. In fact, in the Irish power system, the POR triggers within 5 s from the start of the disturbance and remain in operation for up to 15 s [42]. Indeed, these results identify that this kind of response is too late to maintain system frequency dynamics within a safe margin at 75 % wind power generation. However, as shown, the IR controller slows down the rate at which system frequency drops. Thus it increases the time required for the frequency to reach the nadir and allows enough time for the remaining online synchronous generators to actively contribute to the system frequency containment. This is obvious from the HWLI dispatch as illustrated, the time to nadir increased from 3.13 s in Case A to 4.9 s in Case D. Thus it can be concluded that the availability of FFR service from IDCs plays a dominant role in maintaining frequency stability following the outage of LSI, by offsetting the impact of faster system dynamics.

The aggregated power dispatch from all IDC resources in response to the considered disturbance for all case studies are compared in Fig. 8. These graphs illustrate constraints applied on the IDC maximum power dispatch for the low wind dispatch NWHI and the high wind dispatch HWLI while the remaining two dispatches are middle-ground and their response trajectories are similar. As shown, the response from IDC IT

loads is coordinated with the UPS systems using the formerly mentioned parameters (i.e., T_R , dp/dt , and T_{FFR}). It should be noted that, once the IDC IT loads are activated, they follow a constant trajectory and sustain for the complete duration of the event. In contrast, the UPS systems are equipped with dynamic droop mode that continuously tracks system frequency deviations for any variation outside the deadband limits. This means that the rate of power change (dp/dt) mainly depends on the controller time constants and specified gains in response to the system frequency deviation.

As demonstrated from these graphs, the capability of DR units participating in the FFR service is constrained by the maximum availability of delay-tolerant workloads which was set to 100 MW. Thus, in all dispatches, the DR units reduce quickly and sustain at -100 MW in order to minimize stress on the contribution required from the UPS systems. However, since IT loads do not suffice to offset the impact of the disturbance totally, the UPS systems have issued a small amount of response that reached 125 MW to further compensate the power deficit (e.g., dispatch LWHI). It is to be noted that, in dispatch HWLI, the capability of droop-based synchronous generators is insufficient to actively arrest system frequency. Thus, the UPS systems are required to provide higher energy for a longer duration in order to maintain frequency dynamics and to relieve the impact of generation reserve deficiency. Nevertheless, due to constraints applied on the UPS dispatched power, the maximum limit of 250 MW is reached for up to 5 s, as demonstrated in Case B. It is worth noting that stress on this limitation is reduced to 2 s when the IT loads are joint with the UPS systems, as in Case C.

5.1.2. Effect of IDC response on RoCoF

This sub-section investigates the impact of different wind power operational dispatches on the system frequency RoCoF with and without an FFR service. It is worth noting that all RoCoF values are considered after they are filtered over a timeframe of 500 ms to be consistent with current grid code regulations [53]. As shown in Fig. 9, for the same disturbance, reducing system inertia has resulted in significantly higher RoCoF values. As an example, the maximum absolute RoCoF has increased considerably, from 246 mHz/s in NWHI dispatch to 1004 mHz/s when the power system operational dispatch has changed to HWLI. Nevertheless, with the help of a fast responding of the UPS or DR units, power can be delivered to effectively mitigate the RoCoF. Comparing the bar charts A, B, and C, it is obvious that the activation of IDC resources has very little impact on the maximum RoCoF for the LWHI dispatch. This is due to the fact that initially the system inertia is high and the maximum RoCoF is primarily low. However, the positive impact of the IDC resources is significantly larger when the penetration of wind power is high (e.g., HWLI dispatch), thus enhancing the

usefulness of the service. As an example, the absolute maximum RoCoF has reduced from 1004 mHz/s in Case A to 887 mHz/s in Case B. This change is due to the direct impact of the UPS energy flow on the system frequency during the timeframe of the inertia response which is limited to less than 300 ms from the time when the event began.

Unsurprisingly, activation of DR units does not contribute toward the RoCoF improvement considerably. This is due to the relatively smaller magnitude of the IT loads as well as the time delay included with their communication and actuation response. In this analysis, DR units are set to respond within 250 ms from the start of the disturbance and reach full active power within 2 s to fulfill the requirements of FFR service in Ireland [14]. These results justify the findings in our previous work that the RoCoF cannot be impacted if the DR units are responded after 300 ms [10]. Currently, the post-contingency RoCoF is limited to ± 500 mHz/s measured over a window of 500 ms across the All-Island power system [53]. However, the TSO of Ireland had planned for the RoCoF limit to be increased to ± 1000 mHz/s by the end of 2017, but this level is still in the trial process and yet not officially implemented [42]. Obviously, the maximum RoCoF limit of 500 mHz/s is violated in dispatch HWLI as well as in dispatch MWMI during which the IR controller was disabled.

Results obtained from the preliminary analysis of the impact of the proposed IR integrated into the IDC UPS systems are compared in case studies D, E, and F. These bar charts reflect the role of the IR support applied to different wind penetration levels. One important observation is that the impact of virtual IR on the maximum RoCoF is crucial at high wind penetration levels. One can see the effect clearly in dispatch HWLI while comparing Case A with Case D in which the maximum absolute RoCoF has decreased from 1004 mHz/s to 738 mHz/s respectively. Nevertheless, the applied level of IR still cannot offset the RoCoF tolerance of 500 mHz/s for the loss of LSI in dispatch HWLI. The effectiveness of the IR controller was limited in this analysis due to the applied deadband and time delay to the UPS frequency controller. Thus for full compensation, this suggests careful consideration of the controller deadbands as well as the IR controller gain K_{IR} in order to fully offset the impact of reduced system inertia in all areas. Consequently, this would shift the maximum absolute RoCoF to below the line marked as the current RoCoF limit.

5.1.3. IDC impact on tie-line stability

In a real power system, the maximum tie-line flow in both directions has physical limitations that can be sustained without breaching system security rules (i.e., stability, line overloading, and voltage limit, etc.). These limitations are referred to as the total transfer capability of the tie-line. In this analysis, it is assumed that the line loading reaches 100 % if the deviation in power transfer in both directions exceeds 300 MW.

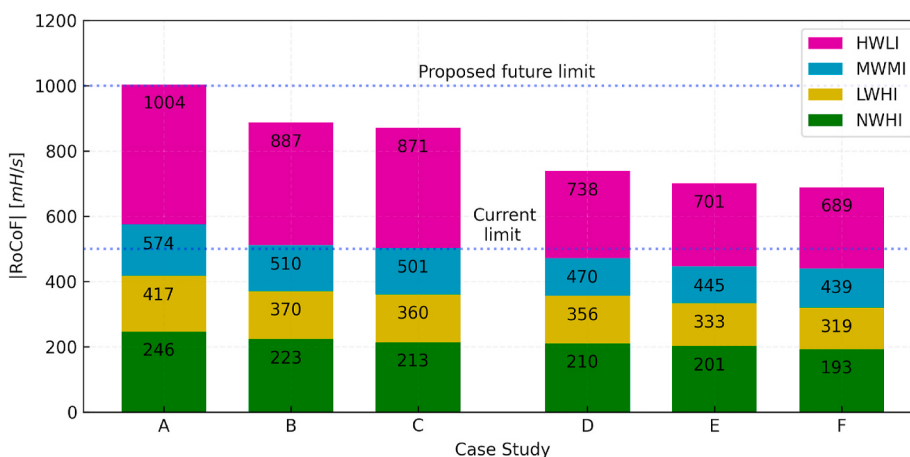


Fig. 9. Maximum absolute RoCoF for various IDC configurations.

Shown in Fig. 10 are power flow deviations in the tie-line 1 that connects Area 1 and Area 2 during different wind power dispatches.

Two important observations can be made from these figures. First, the high wind power generation severely affects the marginal stability of the tie-line interconnection and the maximum power transfer between the areas. This is due to the fact that the governor response of

synchronous generators is gradually reduced to 25 % with the increased penetration of wind power generation to 75 %. It is worth noting that at high wind power generation, under HWLI dispatch, and prior to the full activation of the POR of synchronous generators, small well-damped oscillations are associated with the tie-line power flow. Oscillations in the power began during which kinetic energy of synchronous generators

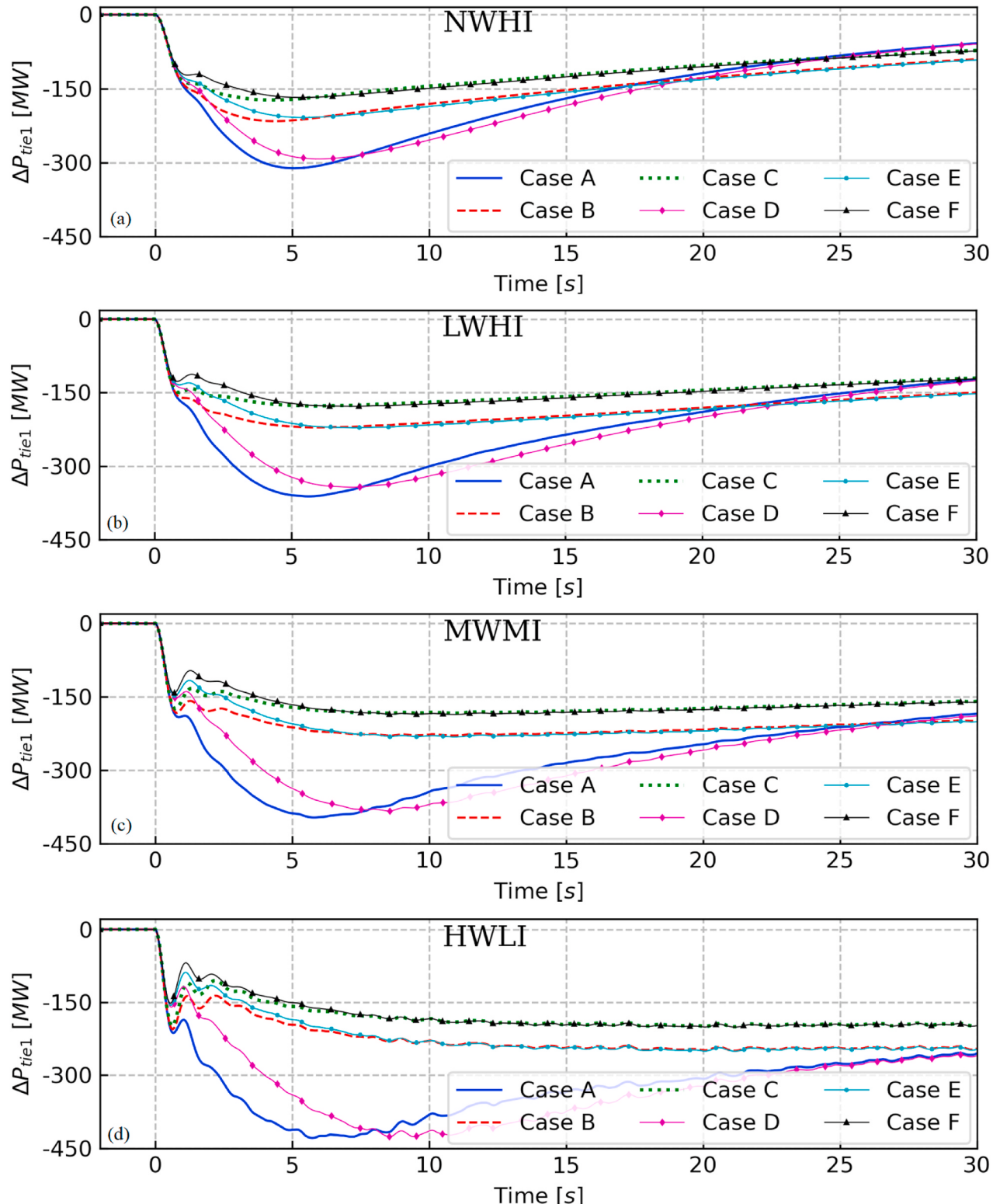


Fig. 10. Tie-line 1 power flow for different dispatches (a) no wind high inertia (NWHI), (b) low wind high inertia (LWHI), (c) medium wind medium inertia (MWMI), and (d) high wind low inertia (HWLI).

is released to cover the lost generation during the disturbance. The angular velocities of conventional generator rotors drop when the POR service is triggered. The system is more susceptible to these oscillations with the increased level of wind penetration and reduced amount of system inertia. This can clearly be seen in Fig. 10 and similar justifications can be made for power flow in line 2 in Fig. 11.

It is also obvious from Fig. 10, that the maximum line loading is breached for all wind operational dispatches. For instance, the maximum change in the value of the instantaneous power in the tie-line reached 300 MW under dispatch NWHI Case A while this value has increased by almost 35 % to 400 MW during the HWLI dispatch Case A. The maximum line loading is sustained for the complete duration of the FFR service, and this rate is gradually reduced following the activation of the POR service. The difference in the line power deviations during the recovery period in HWLI dispatch is slightly under the line loading limit. However, it is still 50 MW higher when compared to the NWHI dispatch. This has resulted from the slow activation of the system spinning reserve in Area 2, and Area 3 to neutralize the disturbance in Area 1. In contrast, the percentage of power loading in line 2 remains

similar during different dispatches, as in Fig. 11.

The second important observation to be made from these analyses is that the proposed IDC framework can effectively handle the impact of the high wind power generation on tie-line stability. It is essential to note that the fast response from the UPS system can highly improve the initial power deviation in the line. As shown in Fig. 10 in Case B, the FFR from the UPS system arrests the line loading well below the permissible limit at 165 MW for all wind dispatches.

Furthermore, the joint response from the UPS with DR loads stabilizes power flow in the tie-line throughout the timeframe of the POR reserve. Again, as the DR units remain offline for a longer duration, the stress on the tie-line power flow can be highly combated. The significance of the proposed framework appears at HWLI as the IDC relives the impact of the lost power during the disturbance and stabilizes the power flow quickly at the very beginning of the event. As an example, the maximum power transfer in tie-line 2 in dispatch HWLI Case A reached 170 MW which decreased to nearly 65 MW in Case Study B and less than 60 MW in Case C. Then the tie-line power flow slowly decreases to its pre-disturbance scheduled value and later during the SOR service the

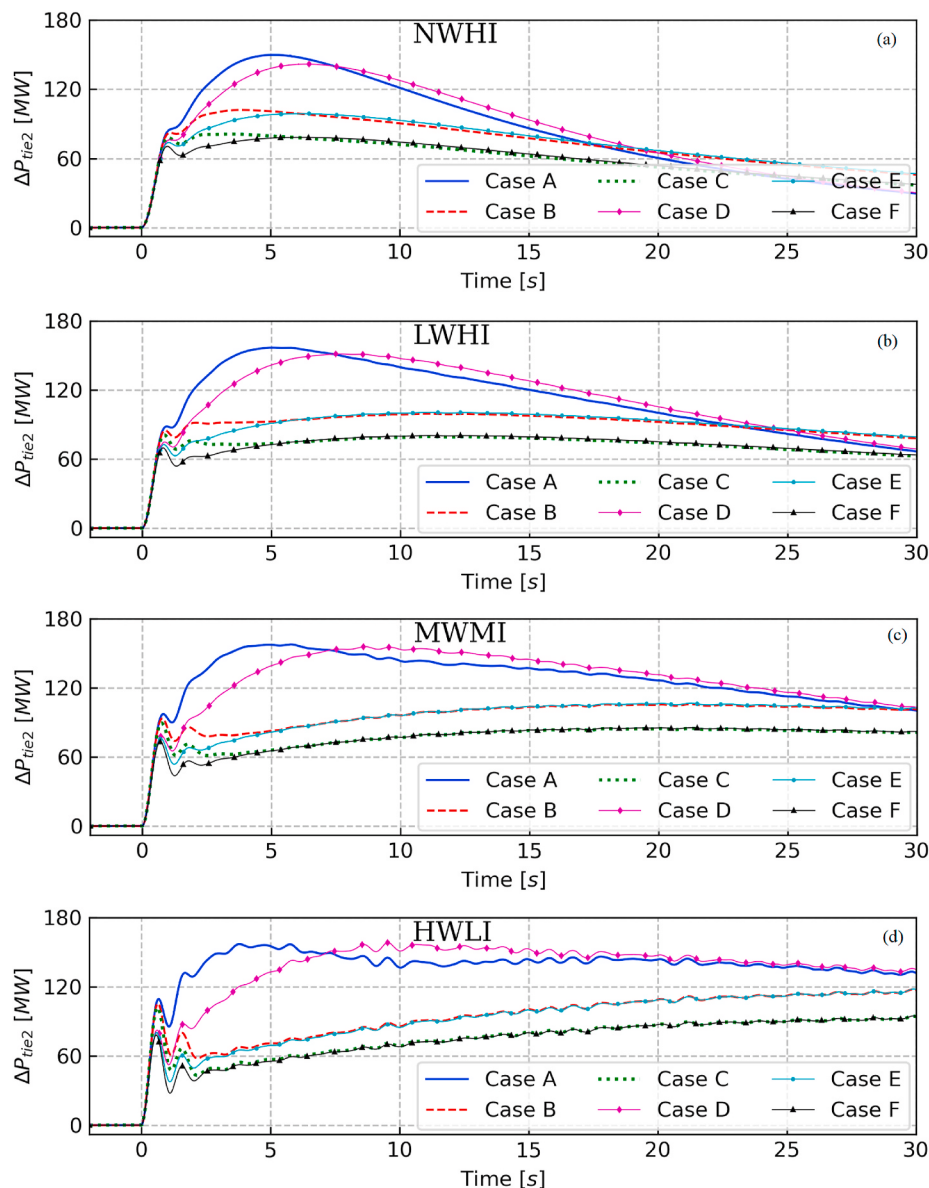


Fig. 11. Tie-line 2 power flow for different dispatches (a) no wind high inertia (NWHI), (b) low wind high inertia (LWHI), (c) medium wind medium inertia (MWMI), and (d) high wind low inertia (HWLI).

LFC regulator starts to re-establish the required power in Area 1.

However, it is to be noted that the IDC response has less impact on the trajectory and the initiated oscillations during the first 2 s due to the delayed response from IDC units. This demonstrates the system need for RoCoF controller and faster response, especially at HWLI operational dispatch. This is obvious from graphs D, E, and F that reveal the tie-line power flow exhibits lower oscillations and less stress with the IR support. An example of this can be seen under HWLI dispatch Case A when compared to Case D during the first second prior to the full activation of FFR service. The maximum instantaneous power transfer in line 2 reached 100 MW and 75 MW respectively.

5.2. Potential resilience benefits from IDC during cascading system failures

This part of the analysis was conducted to stress the performance of the proposed IDC framework under uncertainties associated with wind power generation as well as under cascading system failures. It is supposed that the grid is operating at LWHI dispatch and the wind farms are subject to uncertainties due to the wind speed fluctuations. The variations are assumed to be distributed equally among the wind farms in each area. It is to be noted that constraints on the synchronous generator reserve in each area remain at 75 % of the LSI loss (i.e., 500 MW). Indeed, this reduces the online reserve capability to maintain frequency

stability during non-credible cascade failures. In this research, the disturbance considered is the loss of triple infeeds in Area 1 and Area 2. The first disturbance applied is the trip of HVDC importing a 500 MW at 30 s. This has resulted in almost simultaneous unexpected trips of two wind farms operating at 320 MW and 180 MW in Area 1 and Area 2 respectively, 30 s later. These events resulted in a cumulative level of 1 GW power loss which is greater than the level required to be secured by the current security standards [42]. This kind of disturbance could present frequent future wind farm trips. Three case studies are examined to evaluate the capability of the IDC resources to offer the FFR service during severe cascaded failures:

- Case A: No IDC support
- Case B: UPS as a source of FFR service
- Case C: UPS joint with sustained IT loads as a source of FFR service

System frequency profiles for both incidents are shown in Fig. 12a with and without FFR support from IDCs. As illustrated in Case A, when there is no support from IDCs, system frequency drifted downward to 49.3 Hz and below 49.1 Hz during the first and the second disturbances, respectively. These are extremely low frequency dips that could breach the STAR protection relay in the Irish power system. It is noteworthy that due to the high spinning reserve in Area 1, system frequency recovered back successfully after the first incident. Nevertheless, the

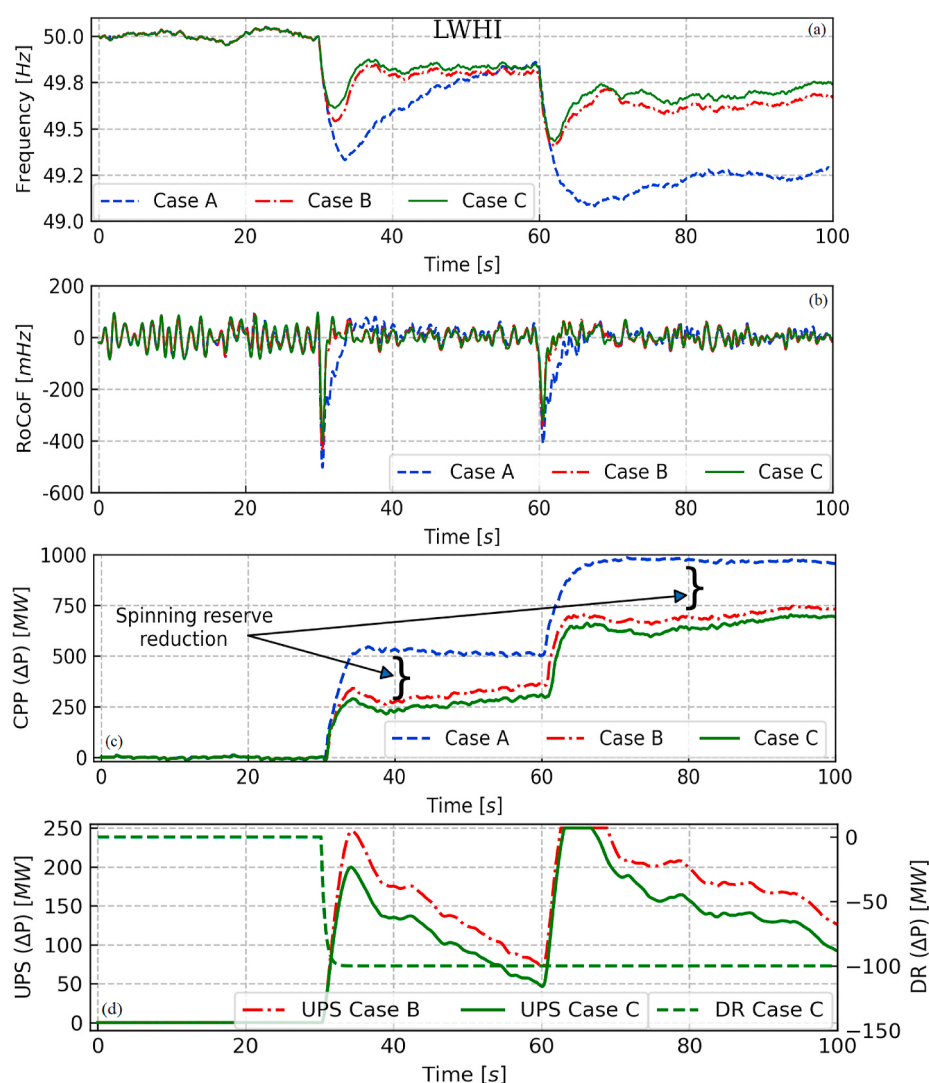


Fig. 12. System dynamics during dispatch LWHI (a) system frequency, (b) RoCoF, (c) conventional power plant response (d) aggregated UPS and DR response.

frequency was not able to run through the second disturbance and remained fluctuating below the STAR protection limit at 49.2 Hz.

In Case Study B, it is supposed that data centers can participate with 250 MW based on their UPS systems only, while in Case C both the UPS and 100 MW IT loads are participating in the FFR service. As shown, even with the presence of uncertainties, the IDC resources could quickly arrest system frequency decline above 49.62 Hz and 49.45 Hz during the first and the second disturbances, respectively. Furthermore, the impact of IT loads on the system frequency deviation is higher during the post-contingency period due to the sustained response of the IT loads over the course of POR. The results indicate that 350 MW IDC resources could maintain the frequency well above the STAR scheme, thereby avoiding possible UFLS protection activation. The trace of system RoCoF for the three studied cases and for the complete duration of the simulation is also depicted in Fig. 12b. It is important to note that the RoCoF measurements are filtered and averaged over a window of 500 ms. As illustrated the uncertainties with wind power fluctuations result in large RoCoF values prior to the activation of the FFR controller. However, these variations are significantly diminished later when the FFR service is triggered. It is also worth noting that the joint participation of the IDC resources has combated the maximum RoCoF by more than 100 mHz/s during each disturbance.

The dynamic behavior of IDC resources following the cascade system failure and in the presence of high wind uncertainties is shown in Fig. 12d. Initially, it is assumed that the IDC power consumption does not change significantly over the short period of 30 s prior to event initiation and thus the (ΔP_{DR} and $\Delta P_{UPS} = 0$). Typically, IDCs have load profiles that are classified as flat because of the high average daily load factor (e.g., 98 %) which indicates flat short-term loads [21]. As can be seen, the power consumption of the modeled IDC loads has started to reduce immediately within 2 s from the start of the event providing 100 MW from their maximum power consumption. Similarly, once the UPS systems are triggered, their power consumption has changed dynamically in proportion to the frequency variations. The maximum dispatched power is reached when the system frequency deviates below 49.5 Hz. Importantly, the FFR service was fully delivered before the full activation of the POR of synchronous generators. This is an essential property of the FFR service to bridge the gap between the inertia response service and the POR service, which can help the system operate securely at high wind power generation. This feature would allow less use of the slower POR and a faster way to arrest frequency nadir too far

from 50 Hz. Shown in Fig. 12c the aggregated output power for all generators in the three areas of the power system. It is obvious that the use of IDC resources has significantly reduced the requisite online spinning reserve from conventional power plants by more than 25 % during each incident.

5.3. IDC impact on system frequency response under signal delays

This subsection examines the impact of delay times on the system frequency response and RoCoF for both the NWHI and HWLI operational dispatches. These dispatches are chosen to present two areas of concern including excessive time delay within the control loop and high penetration of non-responsive wind power generation. It compares the well interconnected strong scenario with the most sensitive and fragile network due to the limited availability of synchronous inertia. From the practical point of view, IDCs cannot respond to trigger signals immediately and there exist delays in the process. Thus extensive assessments have been conducted to examine the potential benefits from the FFR service under a wide range of degraded responses that may occur due to latency and communication jitters. For the purpose of this study, six different emulated delay (T_d) times (e.g., 200 ms, 400 ms, 600 ms, 800 ms, and 1000 ms) are introduced to the model.

Fig. 13 depicts an example of system frequency response for the NWHI operational dispatch under different delay signals. It is to be noted that due to the high synchronous inertia response, system frequency drops slowly and reaches a nadir of 49.56 Hz after 4.3 s. Thus any IDC response during the early stage of this time widow can still have a detrimental impact on the severity of frequency deviations. As shown, for delay times up to 1 s, the system frequency is maintained above 49.69 Hz. It is also essential to note that the fast response of the IDC units does not introduce oscillations during the quasi-steady state frequency recovery. Nevertheless, for all delay values, the FFR service shows a little or no detrimental impact on the maximum RoCoF. It is noteworthy, that at high delays maximum RoCoF is indistinguishable and thus the sensitivities to late response become meaningless.

Noticeably, at HWLI operational dispatch, increasing time delays in the remote signals escalate the severity of the frequency nadir, RoCoF, and quasi-steady-state frequency. As can be seen from Fig. 14, the participation of IDC resources can significantly improve system frequency deviations for different amounts of time delays up to 600 ms. However, the frequency nadir drifts downward close to the originally

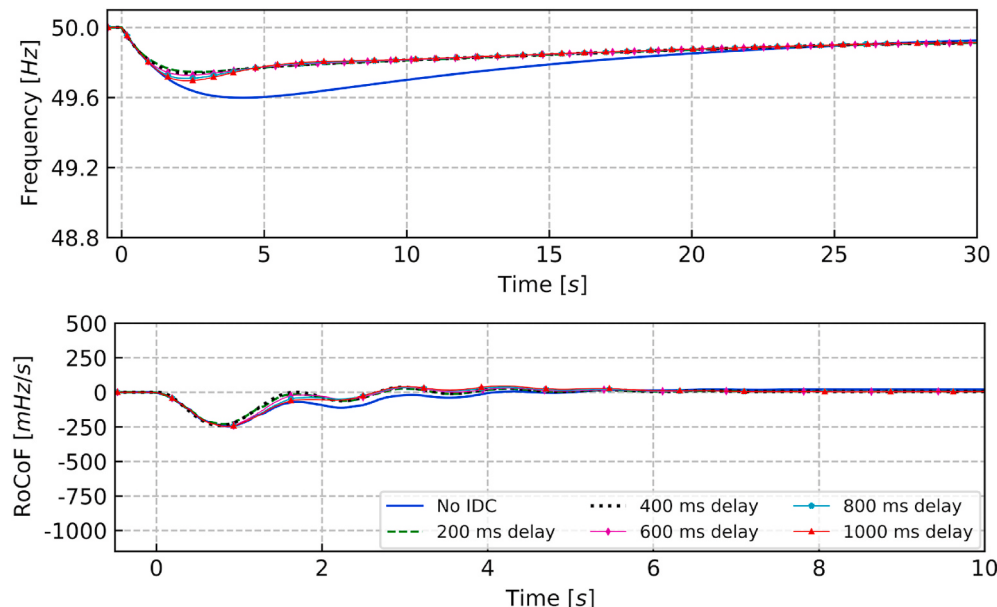


Fig. 13. System frequency response for NWHI dispatch with different delay signals.

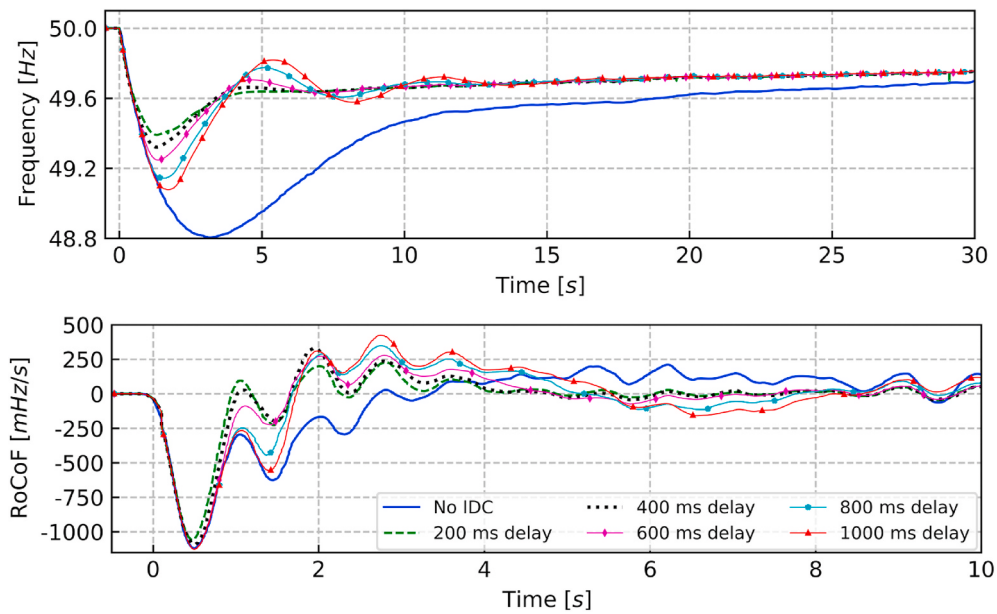


Fig. 14. System frequency response for HWLI dispatch with different delay signals.

initiated disturbance if IDCs responded later than 1000 ms. Similarly, as results indicate the longer delays behind 200 ms, the FFR scheme has very little impact on the maximum initiated RoCoF. As an example, for delay times of 200 ms and 400 ms, the maximum absolute RoCoF has reduced from 1000 mHz/s to 740 mHz/s and 933 mHz/s respectively. It is essential to note that for any delay values behind 400 ms, the scheme has no impact on the severity of RoCoF.

It is noteworthy that the slow response of the IDC behind 400 ms has introduced frequency oscillatory behavior. The impact of these oscillations can clearly be seen from the trace of frequency during the recovery period while the delay time is 1000 ms. As shown, the post-disturbance subsequent frequency oscillation has changed between 49.75 Hz and 49.57 Hz and it is completely damped after 13 s. The impact of these oscillations can also be seen from the variation of RoCoF within 3 s following the time of disturbance began. Although the proposed FFR based MPC method has shown to be able to reject frequency oscillations and disturbances for up to 1000 ms delays, under unfavorable conditions, these kinds of responses may lead to complete system instability. Thus the results are evidence that the currently imposed requirements on the FFR service may not be able to guarantee secure operation of the power system at 75 % SNSP if the level of inertia is significantly reduced. The analysis suggests that to ensure the safe operation of synchronously isolated power systems with high wind penetration, it is essential for the FFR scheme to employ a very quick response, less than 200 ms, to maintain frequency nadir and RoCoF within permissible ranges. These findings are in an agreement with our analysis for the FFR scheme in Ref. [10].

5.4. Limitations of the analysis

This research has done a broad sweep across several aspects related to the IDC utilization for the FFR service. However, a number of assumptions have been made due to the difficulty of accessing real-time power consumptions of actual IDCs. This is because, technical data related to IDC are typically treated in a highly confidential manner, and not disclosed for public research purposes. Therefore, in this analysis, it is assumed that each IDC will be equipped with multiple newly designed bi-directional UPS technologies to supply power back to the grid during disturbances. Furthermore, it is also presumed that the EMS implements the FIFO policy in accordance with the system operator to schedule server jobs during the frequency event without violating the SLA.

Considering these assumptions, a centralized FFR framework is developed in MATLAB/SIMULINK, with two aggregators each containing six DR control blocks and six large UPS units. However, much more power engineering analysis is still required to see something like this applied to real power systems. Fundamental research analysis will be needed to establish suitable data architecture to monitor and control aggregated IDC resources for the FFR service.

6. Conclusions

In this work, a centralized framework was developed for IDCs to participate in a newly developed FFR service in islanded power systems. In the proposed model a novel joint participation of the UPS systems, and delay-tolerant IT workloads were presented to deliver both IR and FFR services in accordance with the grid frequency support. In addition, the concept of the MPC method was utilized to produce reference signals for the IDC resources while respecting device constraints (e.g., maximum power limit, ramp rate, and response time). The potential impact of IDCs on the important frequency response metrics (i.e., RoCoF, frequency nadir, time to nadir, and settling frequency) were extensively examined using a range of wind generation dispatches for 2030. Uncertainties due to the wind power variability, system inertia reduction, and response delays associated with communication and device actuation were also analyzed.

The simulation results depicted that the joint participation of 350 MW IDC resources can provide superior performance in mitigating the severity of frequency deviation and tie-line power flow in ultra-low inertia systems. It was demonstrated that frequency deviation and RoCoF could be arrested above 49.6 Hz and below 730 mHz/s respectively while facilitates secure operation at 75 % SNSP. The analysis identified that in low inertia systems, the current practice of scheduling 75 % of LSI as POR service are no longer guarantees system security. This is due to the anticipated cascaded system failures which may occur when operating at high wind generation. Nevertheless, with the proposed scheme, it was shown that the requirements for the spinning reserve of synchronous machines could be reduced extensively while ensuring frequency deviation remain near 49.5 Hz during cascaded generator trip. The analysis also illustrated that a full control operation of the FFR service should be delivered in a timescale less than 500 ms following generation/load imbalance to provide excellent frequency nadir and RoCoF reductions. The obtained results indicate that a well-

designed, reliable, and fast communication platform is a critical need to deploy a centralized framework and avoid frequency oscillatory behavior during a steady state.

As we incrementally lower the inertia of our power systems and thus problems with synchronous generators are exposed when there are not others to compensate them. Therefore, future implementation of the proposed FFR service from IDCs can be one of many options to help facilitate the integration of higher levels of renewables. However, further research is needed to see which solution is best and will take a holistic approach that looks at the transition across multiple dimensions [54]. Thus in the future, the analysis will examine IDCs from different perspectives (i.e., workload migration). Finally, for better and reliable grid frequency support, the performance of the system will be examined under both fixed and stochastic delay signals using different delay compensation control techniques.

Credit roles

Dlzar Al Kez: Investigation, Writing – original draft, Visualization. Aoife M. Foley supervision, Conceptualization, Investigation, Writing – review & editing, Funding acquisition. Faraedoon W. Ahmed: contributed to the modelling and simulations. Mark O’Malley and S. M. Muyeen: Conceptualization, reviewing & editing.

Declaration of competing interest

The authors declare that they have no known competing financial interests or personal relationships that could have appeared to influence the work reported in this paper.

Acknowledgments

This work is part of the Collaborative REsearch of Decentralization, Electrification, Communications and Economics (CREDENCE) project, which is funded by a US-Ireland Department for the Economy (DfE), Science Foundation Ireland (SFI) and a US National Science Foundation (NSF) award under the Research and Development Partnership Program (Centre to Centre) award (grant number USI 110). The views and opinions expressed in this paper do not necessarily reflect those of the DfE, SFI, and NSF.

References

- [1] Carroll R. Why Ireland’s data centre boom is complicating climate efforts. The Irish Times; 2020. <https://www.irishtimes.com/business/technology/why-ireland-s-data-centre-boom-is-complicating-climate-efforts-1.4131768>. [Accessed 8 September 2020].
- [2] EirGrid/SONI. All-island generation capacity statement 2019–2028. 2019. Dublin, Ireland.
- [3] Cao X, Zhang J, Poor HV. Data center demand response with on-site renewable generation: a bargaining approach. IEEE/ACM Trans Netw 2018;26:2707–20. <https://doi.org/10.1109/TNET.2018.2873752>.
- [4] Masson-Delmotte V, Zhai P, Pörtner H-O, Roberts D, Skea J, Shukla PR, et al., IPCC. Summary for policymakers. In: global warming of 1.5°C. World Meteorological Organization. 2018. Geneva, Switzerland: 2018.
- [5] Manjola B, Martin J. Renewable technologies in the EU electricity sector: trends and projections - analysis in the framework of the EU 2030 climate and energy strategy. Luxembourg: Publications Office of the European Union; 2017. <https://doi.org/10.2760/43833>.
- [6] Sullivan JO, Rogers A, Flynn D, Member S, Smith P, Mullane A, et al. Studying the maximum instantaneous non-synchronous generation in an island system — frequency stability challenges in Ireland. IEEE Trans Power Syst 2014;29:2943–51. <https://doi.org/10.1109/TPWRS.2014.2316974>.
- [7] EirGrid/SONI. Shaping our electricity future. 2021. Dublin, Ireland.
- [8] AEMO. Notice of South Australia Inertia Requirements and Shortfall. 2020. Australian Energy Market Operator, Australia.
- [9] Wang W, Abdolraslidi A, Yu N, Wong D. Frequency regulation service provision in data center with computational flexibility. Appl Energy 2019;113304:251. <https://doi.org/10.1016/j.apenergy.2019.05.107>.
- [10] Al Kez D, Foley AM, Muyeen SM, Morrow DJ. Manipulation of static and dynamic data center power responses to support grid operations. IEEE Access 2020;8: 182078–91. <https://doi.org/10.1109/access.2020.3028548>.
- [11] Gu H, Yan R, Saha TK, Muljadi E, Tan J, Zhang Y. Zonal inertia constrained generator dispatch considering load frequency relief. IEEE Trans Power Syst 2020; 35:3065–77. <https://doi.org/10.1109/TPWRS.2020.2963914>.
- [12] Zhao X, Xue Y, Zhang X-P. Fast frequency support from wind turbine systems by arresting frequency nadir close to settling frequency. IEEE Open 2020;7:191–202. <https://doi.org/10.1109/OAJPE.2020.2996949>. Access J Power Energy.
- [13] Meng L, Zafar J, Khadem SK, Collinson A, Murchie KC, Coffele F, et al. Fast frequency response from energy storage systems – a review of grid standards, projects and technical issues. IEEE Trans Smart Grid 2020;11:1566–81. <https://doi.org/10.1109/TSG.2019.2940173>.
- [14] EirGrid/SONI. DS3 system services scalar design recommendations paper (DS3 system services implementation project). 2017. Dublin, Ireland.
- [15] Stanojev O, Markovic U, Aristidou P, Hug G, Callaway DS, Vrettos E. MPC-based fast frequency control of voltage source converters in low-inertia power systems. ArXiv:200402442v1 [EessSV] 2020.
- [16] Subramanian I, Member S, Debusschere V. A distributed model predictive control framework for grid-friendly distributed energy resources. Trans Sustain Energy 2021;12:727–38. <https://doi.org/10.1109/TSTE.2020.3018913>.
- [17] Sockeel N, Gafford J, Papari B, Mazzola M. Virtual inertia emulator-based model predictive control for grid frequency regulation considering high penetration of inverter-based energy storage system. IEEE Trans Sustain Energy 2020;11:2932–9. <https://doi.org/10.1109/TSTE.2020.2982348>.
- [18] Bevrani H. Robust power system frequency control. second ed. Switzerland: Springer International Publishing; 2014. <https://doi.org/10.1007/978-3-319-07278-4>.
- [19] Paul D, Zhong WD, Bose SK. Demand response in data centers through energy-efficient scheduling and simple incentivization. IEEE Syst J 2017;11:613–24.
- [20] Cupelli L, Schutz T, Jahangiri P, Fuchs M, Monti A, Muller D. Data center control strategy for participation in demand response programs. IEEE Trans Ind Informatics 2018;14:5087–99. <https://doi.org/10.1109/TII.2018.2806889>.
- [21] Ghatikar G, Piette MA, Fujita S, McKane A, Dudley JH, Radspieler A, Mares KCSD. Demand response and open automated demand response opportunities for data centers. Berkeley, California, United States: Lawrence Berkeley National Lab. (LBNL); 2010. <https://doi.org/10.2172/981725>.
- [22] Koronen C, Åhman M. Data centres in future European energy systems — energy efficiency, integration and policy. Energy Effic 2020;13:129–44. <https://doi.org/10.1007/s12053-019-09833-8>.
- [23] Kau K, Garg S, Kumar N, Member S. An adaptive grid frequency support mechanism for energy management in cloud data centers. IEEE Syst J 2020;14: 1195–205. <https://doi.org/10.1109/JSYST.2019.2921592>.
- [24] Eaton. A new opportunity for data centre power infrastructure. 2020. <http://www.eaton.com/gb/en-gb/products/backup-power-ups-surge-it-power-distribution/backup-power-ups/backup-power-solutions/eaton-upsaar.html>. [Accessed 20 October 2020].
- [25] Alaperä I, Honkapuro S, Paananen J. Data centers as a source of dynamic flexibility in smart grids. Appl Energy 2018;229:69–79. <https://doi.org/10.1016/j.apenergy.2018.07.056>.
- [26] Kraftnät Svenska. Final report pilot project in demand response and energy storage. 2018. SVR 3551, Stockholm, Sweden.
- [27] Al Kez D, Foley MA, Brogan P, John DM. Utilizing data centers for inertia and fast frequency response services. In: 2020 2nd int. Conf. Smart power internet energy syst. Util., bangkok, Thailand; 2020. p. 368–73. <https://doi.org/10.1109/SPIES48661.2020.9243001>.
- [28] Chen M, Gao C, Li Z, Shahidehpour M, Zhou Q, Chen S, et al. Aggregated model of data network for the provision of demand response in generation and transmission expansion planning. IEEE Trans Smart Grid 2021;12:512–23. <https://doi.org/10.1109/TSG.2020.3015475>.
- [29] Ghamkhari M, Wierman A, Mohsenian-Rad H. Energy portfolio optimization of data centers. IEEE Trans Smart Grid 2017;8:1898–910. <https://doi.org/10.1109/TSG.2015.2510428>.
- [30] Almazni S, Dabbagh M, Hamdaoui B, Guizani M, Zorba N. Joint resource scheduling and peak power shaving for cloud data centers with distributed uninterruptible power supply. Washington, DC: IEEE Globecom Work. (GC Wkshps); 2016. p. 1–6. <https://doi.org/10.1109/GLOCOMW.2016.7848946>.
- [31] Brocanelli M, Li S, Wang X, Zhang W. Maximizing the revenues of data centers in regulation market by coordinating with electric vehicles. Sustain Comput Informatics Syst 2015;6:26–38. <https://doi.org/10.1016/j.suscom.2014.03.004>.
- [32] Fu Y, Han X, Baker K, Zuo W. Assessments of data centers for provision of frequency regulation. Appl Energy 2020;115621:277. <https://doi.org/10.1016/j.apenergy.2020.115621>.
- [33] Arnone D, Barberi A, La Cascia D, Sanseverino ER, Zizzo G. Green data centres integration in smart grids: new frontiers for ancillary service provision. Elec Power Syst Res 2017;148:59–73. <https://doi.org/10.1016/j.epsr.2017.03.017>.
- [34] Yang T, Hoyt Y, Lee YC, Ji H, Zomaya AY. Power control framework for green data centers. IEEE Trans Cloud Comput 2020. <https://doi.org/10.1109/tcc.2020.3022789>.
- [35] Basmadjian R. Flexibility-based energy and demand management in data centers: a case study for cloud computing. Energies 2019;12:1–22. <https://doi.org/10.3390/en12173301>.
- [36] McClurg J. Fast demand response with datacenter loads : a green dimension of big data. University of Iowa; 2017.
- [37] Ghatikar G, Ganti V, Matson N, Piette MA, Berkeley L. Demand response opportunities and enabling technologies for data centers: findings from field studies. Lawrence Berkeley National Lab. (LBNL). 2012. Berkeley, California, United States.

- [38] Hong Q, Karimi M, Sun M, Norris S, Bagleybter O, Wilson D, et al. Design and validation of a wide area monitoring and control system for fast frequency response. *IEEE Trans Smart Grid* 2020;11:3394–404. <https://doi.org/10.1109/TSG.2019.2963796>.
- [39] Musleh AS, Muyeen SM, Al-Durra A, Kamwa I, Masoum MAS, Islam S. Time-delay analysis of wide-area voltage control considering smart grid contingencies in a real-time environment. *IEEE Trans Ind Informatics* 2018;14:1242–52. <https://doi.org/10.1109/TII.2018.2799594>.
- [40] Al Kez D, Foley AM, Morrow DJ. A comparative assessment of battery energy storage locations in power systems with high wind power penetrations. In: 2020 IEEE int. Conf. Environ. Electr. Eng. 2020 IEEE int. Commer. Power syst. Eur.. (EEEIC/I&CPS eur. Madrid, Spain: IEEE; 2020. p. 1–6. <https://doi.org/10.1109/EEEIC/ICPSEurope49358.2020.9160566>.
- [41] EirGrid. EirGrid grid code. 2019., Version 8.
- [42] EirGrid/SONI. Operational constraints update 27/01/2021. 2021. Dublin, Ireland.
- [43] Khamies M, Magdy G, Hussein ME, Banakhr FA, Kamel S. An efficient control strategy for enhancing frequency stability of multi-area power system considering high wind energy penetration. *IEEE Access* 2020;8:140062–78. <https://doi.org/10.1109/ACCESS.2020.3012119>.
- [44] Pradhan C, Bhende CN, Srivastava AK. Frequency sensitivity analysis of dynamic demand response in wind farm integrated power system. *IET Renew Power Gener* 2019;13:905–19. <https://doi.org/10.1049/iet-rpg.2018.5602>.
- [45] Cheng L, Chen G, Gao W, Zhang F, Li G. Adaptive time delay compensator (ATDC) design for wide-area power system stabilizer. *IEEE Trans Smart Grid* 2014;5: 2957–66. <https://doi.org/10.1109/TSG.2014.2347401>.
- [46] Hui H, Ding Y, Song Y, Rahman S. Modeling and control of flexible loads for frequency regulation services considering compensation of communication latency and detection error. *Appl Energ* 2019;250:161–74. <https://doi.org/10.1016/j.apenergy.2019.04.191>.
- [47] Hosseini SA, Toulabi M, Dobakhshari AS, Ashouri-Zadeh A, Ranjbar AM. Delay compensation of demand response and adaptive disturbance rejection applied to power system frequency control. *IEEE Trans Power Syst* 2020;35:2037–46. <https://doi.org/10.1109/TPWRS.2019.2957125>.
- [48] Abdulrahman I, Radman G. Wide-area-based adaptive neuro-fuzzy SVC controller for damping interarea oscillations. *Can J Electr Comput Eng* 2018;41:133–44. <https://doi.org/10.1109/CJECE.2018.2868754>.
- [49] Wu X, He J, Xu Y, Lu J, Lu N, Wang X. Hierarchical control of residential HVAC units for primary frequency regulation. *IEEE Trans Smart Grid* 2018;9:3844–56. <https://doi.org/10.1109/TSG.2017.2766880>.
- [50] Dozein MG, Member S, Jalali A. Fast frequency response from utility - scale hydrogen electrolyzers. *IEEE Trans Sustain Energy*; 2021. <https://doi.org/10.1109/TSTE.2021.3063245>.
- [51] O'Sullivan JW, O'Malley MJ. Economic dispatch of a small utility with a frequency based reserve policy. *IEEE Trans Power Syst* 1996;11:1648–53. <https://doi.org/10.1109/59.535710>.
- [52] O'Sullivan JW, O'Malley MJ. A new methodology for the provision of reserve in an isolated power system. *IEEE Trans Power Syst* 1999;14:519–24. <https://doi.org/10.1109/59.761875>.
- [53] EirGrid/SONI. ReCoF alternative & complementary solutions project. 2016. Dublin, Ireland.
- [54] Global PST Consortium. Inaugural research agenda. 2021.